Check for updates

Evaluating the techno-economic potential of defossilized air-to-syngas pathways†

Hussain M. Almajed, [ab] Omar J. Guerra, [c] Wilson A. Smith, [abcd] Bri-Mathias Hodge [⋆bcef] and Ana Somoza-Tornos [⋆bd]

Defossilizing the chemical industry using air-to-chemical processes offers a promising solution to driving down the emission trajectory to net-zero by 2050. Syngas is a key intermediate in the chemical industry, which can be produced from electrolytic H_2 and air-sourced CO_2. To techno-economically assess possible emerging air-to-syngas routes, we develop detailed process simulations of direct air CO_2 capture, proton exchange membrane water electrolysis, and CO_2 electrolysis. Our results show that renewable electricity prices of ≤$15 per MW h enable the replacement of current syngas production methods with CO_2 electrolysis at CO_2 avoidance costs of about $200 per t-$CO_2$. In addition, we identify necessary future advances that enable economic competition of CO_2 electrolysis with traditional syngas production methods, including a reverse water gas shift. Indeed, we find an improved CO_2 electrolysis process (total current density = 1.5 A cm^{-2}, CO_2 single-pass conversion = 54%, and CO faradaic efficiency = 90%) that can economically compete with the reverse water gas shift at an optimal cell voltage of about 2.00 V, an electricity price of $28–42 per MW h, a CO_2 capture cost of $100 per t-$CO_2$, and CO_2 taxes of $100–300 per t-$CO_2$. Finally, we discuss the integration of the presented emerging air-to-syngas routes with variable renewable power systems and their social impacts in future deployments. This work paints a holistic picture of the targets required to economically realize a defossilized syngas production method that is in alignment with net-zero goals.

Broader context

Climate change has already caused increases in heat waves, wildfires, and sea levels worldwide. With increasing global CO_2 emissions reaching an all-time-high of more than 36.8 Gt-CO_2 in 2022, the world is furthering away from net-zero emission targets. Along with energy decarbonization efforts, CO_2 capture from point sources and air plays a significant role in driving the trajectory down to the net-zero emission point by mid-century. Air-to-product processes offer defossilized pathways to pursue carbon neutrality while benefiting from economic incentives. To date, there has been a lack of rigorous modeling and techno-economic studies on emerging air-to-syngas pathways. The present work aims to fill that gap by providing a thorough assessment of integrating direct air CO_2 capture (DACC) with CO_2 and H_2O electrolysis systems to produce syngas, a key intermediate in the chemical industry. A comparison of such an emerging route with traditional ones is given to guide further DACC-electrolysis research towards relevant targets. In addition, we provide carbon pricing targets, integration with variable renewable energy considerations, and social implications of deploying such pathways, composing a comprehensive overview of upcoming challenges to stakeholders.

[a] Department of Chemical and Biological Engineering, University of Colorado Boulder, Boulder, CO 80309, USA

[b] Renewable and Sustainable Energy Institute, University of Colorado Boulder, Boulder, CO 80309, USA. E-mail: A.SomozaTornos@tudelft.nl, BriMathias.Hodge@colorado.edu

[c] National Renewable Energy Laboratory, Golden, CO, 80401, USA

[d] Delft University of Technology, Department of Chemical Engineering, Van der Maasweg 9, 2629 HZ Delft, The Netherlands

[e] Department of Electrical, Computer and Energy Engineering, University of Colorado Boulder, Boulder, CO 80309, USA

[f] Department of Applied Mathematics, University of Colorado Boulder, Boulder, CO 80309, USA

† Electronic supplementary information (ESI) available. See DOI: https://doi.org/10.1039/d3ee02589f

1. Introduction

Global CO_2 emissions hit an all-time-high of more than 36.8 Gt-CO_2 in 2022.[1] Even with accelerated reductions in CO_2 emissions, it is inevitable that the global temperature increase will exceed 1.5 °C (above pre-industrial levels) by 2100,[2] which will cause additional worldwide climate change disasters including but not limited to heat waves, coastal flooding, and wildfires.[2–5] The great uncertainty around how further increases will impact humanity highlights the importance of keeping the increase in global temperature below 2 °C.[6] To accomplish this goal, CO_2-emitting industries must stop emitting CO_2, and further efforts must be

This journal is © The Royal Society of Chemistry 2023

Energy Environ. Sci., 2023, **16**, 6127–6146 | 6127

devoted to removing greenhouse gases permanently from the atmosphere to offset human-generated CO_2 emissions from other sectors.

Out of the 36.8 Gt-CO_2 emitted in 2022, about 8 Gt-CO_2 came from the transportation sector,[1] which currently relies heavily on hydrocarbon fuels. Ideally, decarbonizing the transportation sector using renewably-driven electric vehicles (EVs) or using hydrogen-fueled (H_2-fueled) vehicles would reduce the annual 8 Gt-CO_2 contribution substantially. However, continued human reliance on carbon-based products would also require defossilizing the chemical industry, and sourcing the carbon from non-fossil feedstocks (e.g., air, sea/oceanwater, and biomass). Therefore, chemical and fuel production pathways that encourage a circular carbon economy, a decarbonized energy sector, and a defossilized chemical industry should be pursued to help in limiting the global temperature increase to ≤ 2 °C.

Several reports[6–8] deem that point-source CO_2 capture (PSCC) and carbon dioxide removal (CDR) technologies will play a significant role in pursuing a net-zero emission world. PSCC technologies have been well studied and adopted commercially in several regions of the world (e.g., in Saudi Arabia, the United States, Australia, and China).[9–11] On the other hand, CDR technologies, including bioenergy with carbon capture and storage (BECCS) and direct air CO_2 capture (DACC), have not been adopted commercially yet. Their technology readiness levels (TRLs), based on the definition given by the international energy agency (IEA), range from 1 to 6, with ocean alkalinization and enhanced weathering being at a TRL of 1–3 and BECCS and DACC being at a TRL of 6.[7] BECCS offers an attractive CO_2 capture cost of $13–120 per t-$CO_2$,[10] however its impacts on food security,[6,12–16] biodiversity,[6,12,14–16] crop prices,[12,13] deforestation,[14] and human rights[6,16] raise concerns about its deployment at large scales. DACC can overcome such challenges by offering modular designs,[17–19] low to no competition with food lands,[20,21] and flexible locational possibilities.[19–21] However, its wide literature projected cost range of roughly $100–1000 per ton of CO_2[22] suggests a high uncertainty of the DACC capture cost estimates. In addition, it is generally more expensive than BECCS, largely due to expensive sorbents,[23] high contactor costs,[24] and/or high energy demands for regenerating the captured CO_2 and the solvent/sorbent.[18] Therefore, discovering less-expensive capture materials and improving the DACC process energy efficiency should be targeted to advance DACC towards commercialization. In parallel, however, exploring integration pathways that valorize captured CO_2 is essential in improving the market potential of DACC technologies by creating a product that can be sold to recover at least a portion of the costs.[25]

The two main DACC methods use either a liquid hydroxide solvent or a liquid/solid amine sorbent to capture CO_2 from the atmosphere.[7] Several researchers have reviewed both technologies,[17–19,26] highlighting their benefits and downsides. Solid amine-based DACC can leverage waste heat as an energy supply for the low-temperature (80–120 °C) CO_2 regeneration step. It is also able to capture water along with CO_2 from air using the same solid sorbent, although this can impact the CO_2

capture efficiency and system durability.[27] However, its main weakness is the high cost required to capture CO_2 from the atmosphere ($_{2021}$ 500–600 per t-CO_2), which is mainly due to the specially-designed sorbent as it accounts for about 50% of the total CO_2 capture cost due to its frequent replacement.[17,24] On the other hand, the current state-of-the-art liquid hydroxide-based DACC design uses traditional heat sources (e.g., from burning natural gas) to supply enough heat for the energy-intensive calcination step, which demands an elevated temperature of 900 °C. However, this design leverages already-commercialized equipment and technologies that are manufactured at scale today, reducing the total capture cost estimate to $_{2016}$ 94–232 per t-CO_2,[28] with the minimum cost representing an optimistic scenario (electricity price = $30 per MW h, capital recovery factor = 7.5%, plant = mature plant; TRL 11).

Regardless of the capture method, the captured and regenerated CO_2 can either be stored or converted into higher-value products. Both end uses are essential for reducing emissions while pursuing carbon neutrality.[29] Storing CO_2 in geological formations enables the pursuit of net-zero emission targets. However, existing policies that incentivize storage of the captured CO_2 do not sufficiently cover the cost of most DACC plants today. A quick comparison between today's baseline cost estimates of DACC ($163–1000 per t-$CO_2$) and current carbon incentives, such as the 2022-updated U.S. 45Q tax credit ($180 per t-$CO_{2,stored}$ for DACC[30]) and the European emission trading systems (EU ETS) (Feb. 2023 trading CO_2 price ≈ $100 per t-$CO_2$[31]), illustrates this discrepancy. Utilization of the captured CO_2, on the other hand, allows DACC to cover at least some of its costs while benefiting from increased CO_2 tax credits as an additional revenue stream. Additionally, it could help defossilize the chemical industry by sourcing its carbon feedstock from air instead of fossil fuels.

Several researchers have investigated the integration of CO_2 capture from air with (bi)carbonate and carbamate reductions.[32–37] These pathways eliminate the need for the energy-intensive regeneration step. However, these conversion technologies are still in their early-stage development, suggesting higher uncertainties around their eventual costs and practical performance.[38] CO_2 utilization using both thermochemical and electrochemical methods can overcome this challenge since these technologies are more technologically mature than (bi)carbonate or carbamate reductions today.

Thermochemical and electrochemical CO_2 conversion can produce high-value products such as CO, syngas (i.e., a mixture of CO and H_2), formic acid, methanol, and ethanol. Syngas, in particular, is an essential industrial feedstock for the production of several chemicals and fuels, including methanol, dimethyl ether (DME), ammonia, and Fischer–Tropsch products.[39,40] It is conventionally produced via dry methane reforming (DMR), partial oxidation (POX), and steam methane reforming (SMR) at H_2:CO ratios of 1:1, 2:1, and 3:1, respectively.[39] These processes have a TRL of 8–9, indicating adoption at the commercial scale. Reverse water gas shift (RWGS) is another well-established technology that can produce 2:1 syngas from a feed of CO_2 and H_2, which is commonly

6128 | Energy Environ. Sci., 2023, **16**, 6127–6146

This journal is © The Royal Society of Chemistry 2023

used in methanol synthesis as demonstrated by Joo and co-workers.[41] This technology is implemented in a process called the CAMERE process, which has a TRL of 6–7.[42,43] Depending on the desired syngas ratio, a syngas production method can be selected. For example, an $H_2:CO$ ratio of 2:1 is needed to synthesize Fischer–Tropsch products using cobalt-based catalysts,[44] suggesting POX or RWGS to be the most suitable syngas production methods. However, it is worth noting that the four syngas production methods that are mentioned here require elevated temperatures (≥ 600 °C)[39,45,46] that are currently supplied *via* fossil-based energy sources. Although electrification (*e.g.*, using electric heaters) will play a key role in tackling this issue, the path of the adoption for elevated temperatures of ≥ 600 °C is unclear.[47] Alternatively, the emerging field of CO_2 electrolysis can operate at ambient temperature and pressure, easily utilizing renewable electricity to convert a feed of CO_2 and H_2O into syngas at tunable ratios.

The electrochemical reduction of CO_2 (CO_2ER) to CO at low temperatures (≤ 100 °C) has been extensively investigated.[48–50] The faradaic efficiency towards CO (FE_{CO}), operational stability, CO_2 single-pass conversion, total cell voltage, and total current density are typically used as figures of merit to assess the overall process performance.[25,51] Although low-temperature CO_2ER studies have achieved high FE_{CO} ($\geq 80\%$), high current density (≥ 200 mA cm^{-2}), and moderately low cell voltage (2.5–3.0 V), they have not yet demonstrated sufficient electrolyzer operation stability for industrial implementation (*i.e.*, 44 000 h lifetimes, similar to water electrolysis), and they have not yet achieved all industrial benchmarks concurrently.[25] Indeed, the TRL of low-temperature CO_2ER is in the range of 3–5. Therefore, further assessments of future scenarios can clarify which figures of merit to pursue in a specific context (*e.g.*, for integrated DACC with CO_2 utilization routes).

Although significant research efforts have been devoted to the analysis of integrated carbon capture and utilization, there is still a research gap regarding the process modeling and techno-economic assessment (TEA) of integrated DACC with carbon electrolysis, with only three studies attempting to guide research based on their TEA results. Daniel *et al.*[52] assessed the integration of DACC with a high-temperature (≥ 600 °C) solid oxide electrolysis cell (SOEC) for the production of syngas and found a significant contribution to the capital and operational expenditures (CAPEX and OPEX) from the SOEC due to using large amounts of precious materials and requiring complex manufacturing processes. Their study suggests that the SOEC field should focus on capital cost reductions of the electrolyzer along with energy efficiency improvements. However, the authors focused on an older version of hydroxide-based DACC and on high-temperature CO_2 electrolysis, and they have not considered equilibrium and kinetic factors in their process modeling, which enables advanced physics-based models to improve on their TEA conclusions. Moreno-Gonzalez *et al.*[38] assessed several pathways for producing syngas at an $H_2:CO$ ratio of 2.5, with the goal of comparing the TEA performance of electrochemical pathways to that of a conventional thermochemical one (namely, RWGS). They found no economic competition of gaseous and liquid CO_2 electrolysis with RWGS when integrated with DACC today. However, in a future scenario, in which the performance of CO_2 electrolysis is improved, the authors found both electrolysis pathways to compete economically with RWGS when integrated with DACC. This study also relied on modified literature cost estimates and is not supported by fully integrated process modeling results. In addition, some of the chosen assumptions were inconsistent with state-of-the-art assumptions that are commonly used in the literature. For instance, the authors assumed a proton exchange membrane (PEM) water electrolyzer cost of $600–1500 per kW, which is more than 2.5 times higher than that estimated by the widely-used H_2A production model (*i.e.*, $233–460 per kW).[53] Debergh *et al.*[37] techno-economically assessed the integration of DACC with CO_2 and (bi)carbonate electrolysis systems for 2:1 syngas production. They found DACC integration with (bi)carbonate electrolysis to be more economical than its integration with CO_2 electrolysis, mostly due to minimizing downstream separation and DACC capital costs. However, this claim is dependent on the electricity price as (bi)carbonate electrolysis consumes more electricity (*i.e.*, less energy efficient) than CO_2 electrolysis. In addition, their study did not consider kinetic or equilibrium effects that could influence practical integration of DACC with electrolysis. Indeed, it is still questionable whether the (bi)carbonate electrolyzer is able to regenerate the hydroxides or if additional major equipment is needed to accomplish that step. Thus, thorough TEA studies that are based on rigorous process modeling results, which consider equilibrium and kinetic factors, and that consider realistic assumptions are still absent from the literature of integrated DACC with carbon electrolysis.

Herein, we attempt to fill in that gap by modeling and assessing the integration of a liquid hydroxide-based DACC plant with both a thermochemical and an electrochemical pathway to produce syngas; namely, RWGS and CO_2ER. We consider sourcing the H_2 from PEM water electrolysis (PEMWE) for both routes. However, for the RWGS route, we additionally consider sourcing the H_2 from SMR due to the fact that SMR-RWGS is a well-established integrated process today. Furthermore, we base our process designs on some of the most recent literature, including Keith *et al.*,[28] Rezaei and Dzuryk,[46] and Wen and Ren *et al.*[54] We estimate technical (*i.e.*, carbon efficiency, energy consumption, and marginal energy-associated CO_2 emissions) and economic (*i.e.*, energy cost, capital costs, variable operational costs, fixed operational costs, and total product cost) metrics to compare the current and future states of considered pathways. Additionally, we perform sensitivity analysis on several measures by varying each individually while keeping the others constant at the baseline values. Finally, we investigate the effects of H_2 and electricity prices on the total syngas production cost of both pathways in an optimistic future scenario for the CO_2ER to define research targets that enable the electrochemical pathway to economically compete with RWGS when integrated with DACC. The novelty of the present work is centered around three main points: (i) developing a verified DACC process model in Aspen Plus that considers equilibrium and kinetic interactions, (ii) developing an electrolyzer model that

This journal is © The Royal Society of Chemistry 2023

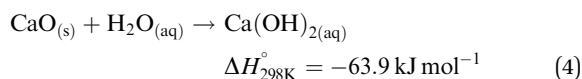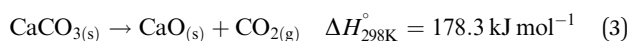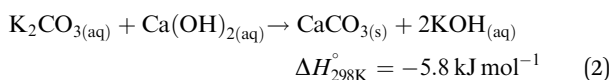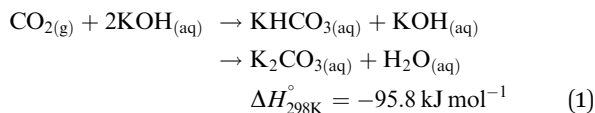*Energy Environ. Sci.*, 2023, **16**, 6127–6146 | **6129**

calculates mass and energy balances and correlates the production rate, current density, and cell voltage together using the simple power and Butler–Volmer equations, and (iii) assessing the economic feasibility of electrochemical and thermochemical pathways when integrated with DACC in several future scenarios. This effort aims to guide future DACC-electrolysis research towards relevant metrics that would significantly improve the techno-economic performance of DACC-CO$_2$ER routes when compared with DACC-RWGS.

2. Process description

2.1. Liquid hydroxide-based direct air CO$_2$ capture (DACC)

The proposal of CO$_2$ capture from air by Lackner *et al.*[55] considered calcium hydroxide as a capture agent due to its high binding energy ($\Delta H^\circ = -109$ kJ mol^{-1})[26] with CO$_2$ and well-established CO$_2$ absorption chemistry. Subsequent work by Zeman and Lackner[56] realized the benefit of integrating calcium looping with solvent regeneration to create a two-cycle process that is able to regenerate the hydroxide solvent and the captured CO$_2$ concomitantly. Today, the state-of-the-art hydroxide-based DACC process design, as developed by Carbon Engineering, uses the same two-cycle process, however with potassium hydroxide as the capture agent due to its higher CO$_2$ absorption kinetics.[28]

The main components of the state-of-the-art process design are the air contactor, pellet reactor, calciner, and slaker (Fig. 1a). The air contactor is the place where CO$_2$ is in direct contact with the hydroxide solvent, allowing the spontaneous formation of (bi)carbonates (eqn (1)). The (bi)carbonates are then fed to the pellet reactor along with a 20% calcium hydroxide slurry (lime) to regenerate the hydroxide-based solvent and form calcium carbonate (eqn (2)). Subsequently, the calcium carbonate is pre-heated in the slaker and fed to the calciner, in which it is decomposed at 900 °C to calcium oxide (quicklime) and concentrated CO$_2$ (eqn (3)). The solid quicklime is co-fed with water to the slaker for lime regeneration (eqn (4)), whereas the gaseous outlet stream, containing the captured CO$_2$, is dehydrated and compressed before storage or transportation. It is worth noting that the calciner takes in a feed of CH$_4$ and O$_2$ for combustion to generate sufficient heat for the calcination (eqn (5)), which reduces the mass composition of CO$_2$ in the gaseous outlet stream.[28]

$$CO_{2(g)} + 2KOH_{(aq)} \rightarrow KHCO_{3(aq)} + KOH_{(aq)}$$
$$\rightarrow K_2CO_{3(aq)} + H_2O_{(aq)}$$
$$\Delta H^\circ_{298K} = -95.8 \text{ kJ mol}^{-1} \quad (1)$$

$$K_2CO_{3(aq)} + Ca(OH)_{2(aq)} \rightarrow CaCO_{3(s)} + 2KOH_{(aq)}$$
$$\Delta H^\circ_{298K} = -5.8 \text{ kJ mol}^{-1} \quad (2)$$

$$CaCO_{3(s)} \rightarrow CaO_{(s)} + CO_{2(g)} \quad \Delta H^\circ_{298K} = 178.3 \text{ kJ mol}^{-1} \quad (3)$$

$$CaO_{(s)} + H_2O_{(aq)} \rightarrow Ca(OH)_{2(aq)}$$
$$\Delta H^\circ_{298K} = -63.9 \text{ kJ mol}^{-1} \quad (4)$$

$$CH_4 + 2O_2 \rightarrow CO_2 + 2H_2O \quad \Delta H^\circ_{298K} = -890.6 \text{ kJ mol}^{-1} \quad (5)$$

2.2. Reverse water gas shift (RWGS)

The RWGS reaction requires a feedstock composed of CO$_2$ and H$_2$ to produce CO and H$_2$O as shown in eqn (6) below.[46,57] The endothermicity of the RWGS reaction, as well as the presence of Sabatier side reactions, as shown in eqn (S5)–(S7) (ESI†), restrict the use of RWGS at low temperatures.[57–59] Thus, temperatures equal to or higher than 700 °C are necessary to increase the CO selectivity in the product stream.[60] Carbon formations are other possible side reactions, eqn (S8)–(S10) (ESI†), that can cause blockage of catalyst active sites, resulting in catalyst degradation, and thus interruption of the RWGS process.[58,59] In addition, CH$_4$ pyrolysis, eqn (S8) (ESI†), is preferred at high temperatures[58] and can compete with the RWGS reaction, eqn (6), strongly.[46]

$$CO_2 + H_2 \leftrightarrow CO + H_2O \quad \Delta H^\circ_{298K} = 42 \text{ kJ mol}^{-1} \quad (6)$$

Since RWGS is a well-established process, we plan to reference an already-built plant simulation. Rezaei and Dzuryk[46] present a thorough process model of a RWGS plant that produces 2:1 syngas from a feed of CO$_2$ and H$_2$. The plant is mainly composed of a RWGS reactor that is operated at 1000 °C, a monoethanolamine (MEA) CO$_2$ absorption setup that recycles unreacted CO$_2$, and some downstream processing steps to arrive at feedstream conditions that are fit for FT-synthesis. Fig. 1b shows the process flow of the considered RWGS plant. For simplicity, Fig. 2 shows only the RWGS reactor.

2.3. Low-temperature CO$_2$ electrolysis

The electrochemical reduction of CO$_2$ can produce a wide variety of products at ambient temperature and pressure, which strongly depends on the used catalyst, reactor configuration, and operating conditions. The selective reduction of CO$_2$ to CO (eqn (7)) is the most technically mature pathway, which can be accomplished using metallic electrocatalysts, such as Ag, Au, and Zn, or molecular electrocatalysts such as Co-pc.[61–63] However, depending on the availability of protons near the cathode, the competing hydrogen evolution reaction (HER), shown in eqn (8), may dominate the catalyst surface, suppressing CO$_2$ER from proceeding forward. Alkaline conditions have shown the ability to relatively suppress the HER, but they favor (bi)carbonate formation (eqn (1)),[64] which would result in CO$_2$ losses that increase the downstream CO$_2$ separation costs. Indeed, embracing the produced H$_2$ might benefit researchers in optimizing for the most relevant performance in the context of syngas production. In other words, aiming for syngas production rather than pure CO production allows CO$_2$ER researchers to focus on improving metrics other than selectivity (FE$_{CO}$), such as CO$_2$ single-pass conversion, which can lower the cost of downstream separation, or operational stability, which can lower both the CAPEX and OPEX of the electrode, catalyst, and membrane replacements. On the anode side, the most common reaction that pairs with cathodic CO$_2$ER is the oxygen evolution reaction (OER), which can use either a Ni electrocatalyst or an IrO$_x$ anode
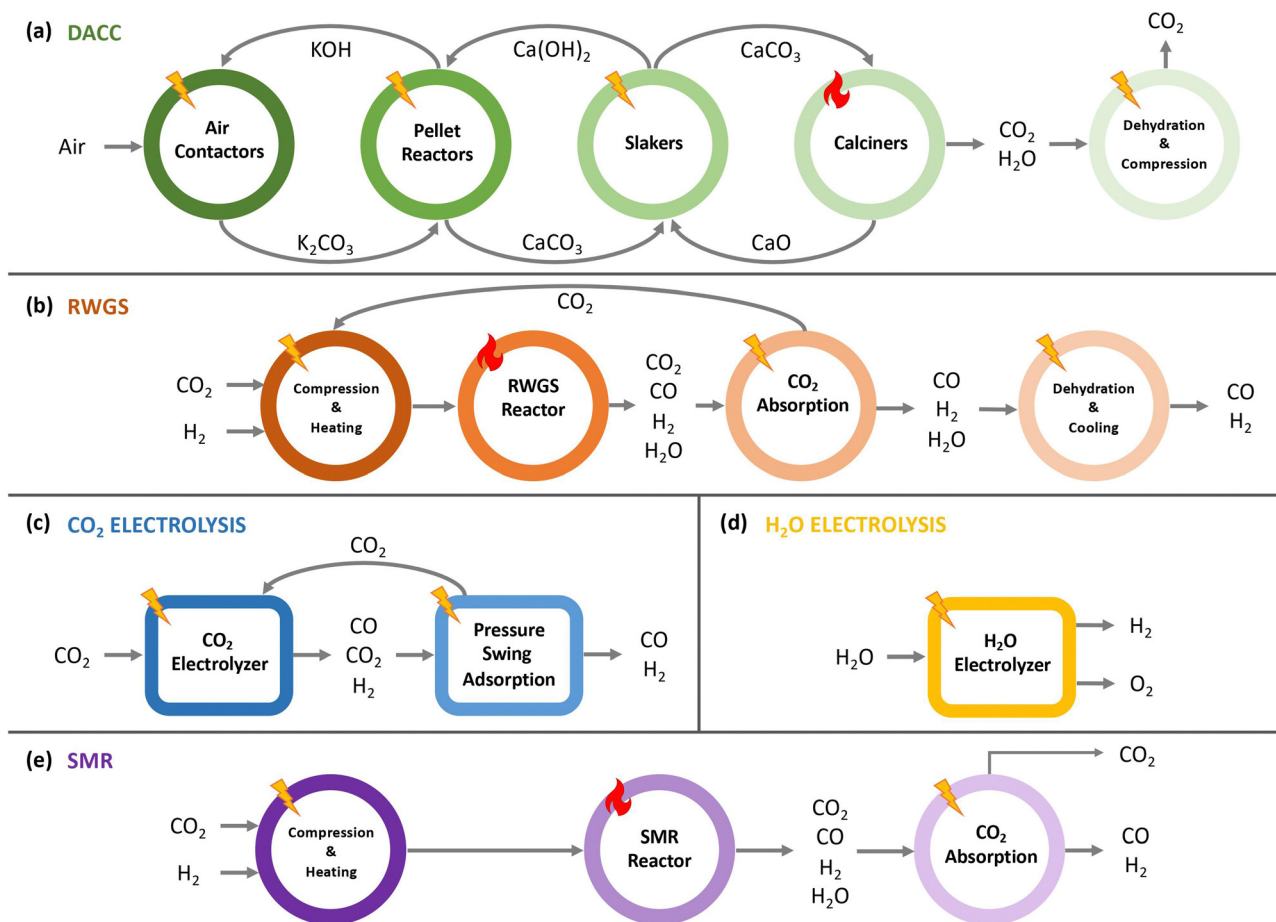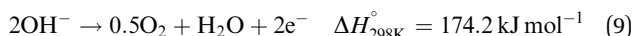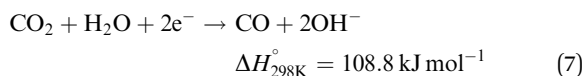
6130 | *Energy Environ. Sci.*, 2023, **16**, 6127–6146

This journal is © The Royal Society of Chemistry 2023

Fig. 1 Simple block flow diagrams of (a) liquid hydroxide–based DACC, (b) reverse water gas shift, (c) CO_2 electrolysis, (d) H_2O electrolysis, and (e) steam methane reforming. The fire symbol represents fossil-based thermal energy and the lightning bolt symbol represents electricity, which can be sourced from renewables.

under acidic conditions (eqn (9)).

$$CO_2 + H_2O + 2e^- \rightarrow CO + 2OH^-$$
$$\Delta H^\circ_{298K} = 108.8 \text{ kJ mol}^{-1} \quad (7)$$

$$2H^+ + 2e^- \rightarrow H_2 \quad \Delta H^\circ_{298K} = 0 \text{ kJ mol}^{-1} \quad (8)$$

$$2OH^- \rightarrow 0.5O_2 + H_2O + 2e^- \quad \Delta H^\circ_{298K} = 174.2 \text{ kJ mol}^{-1} \quad (9)$$

In all low-temperature gaseous CO_2 electrolysis processes, the outlet gas mixture always contains unreacted CO_2 due to the low CO_2 single-pass conversion. Therefore, separating CO_2 from this gas mixture and recycling it back to the reactor is a key step in CO_2 electrolysis. This step can be accomplished by several methods including MEA CO_2 absorption and pressure swing adsorption (PSA), which are both used widely in industry.[51]

Furthermore, a limited number of CO_2ER studies have explored systems and components that target syngas production at a 2:1 H_2:CO ratio as a product.[36,65,66] However, these studies have either not achieved relatively high current densities (≥ 200 mA cm^{-2}) or have used liquid (bi)carbonate as the inlet to the electrolyzer instead of gaseous CO_2. In addition, the focus on co-electrolysis of CO_2 and H_2O to syngas has been on

high-temperature techniques (e.g., SOEC) rather than low-temperature ones. Although SOEC is believed to be a promising technology for CO/syngas production,[67] it is outside the scope of the present study. Thus, we will consider a parallel low-temperature electrolysis of CO_2 and H_2O, in which CO_2 and H_2O are reduced in alkaline and PEM electrolyzers, respectively. To clarify, the two electrolysis processes are performed in separate electrolyzers.

It is worthwhile to mention that there are multiple growing start-up companies that are attempting to scale up low-temperature CO_2 electrolyzers, including twelve,[68] dioxide,[69] and OCO.[70] However, the commercial deployment is yet to be realized, which is why integrated process and techno-economic models that consider industrial scales are needed to push this field forward.

2.4. Water electrolysis

Water electrolysis refers to an electrochemical process in which water is electrochemically converted into oxygen and hydrogen according to eqn (10). The three main commercial water electrolysis technologies are alkaline water electrolysis (AWE), PEMWE, and SOEC.[71] In AWE, the cathode reduces water into
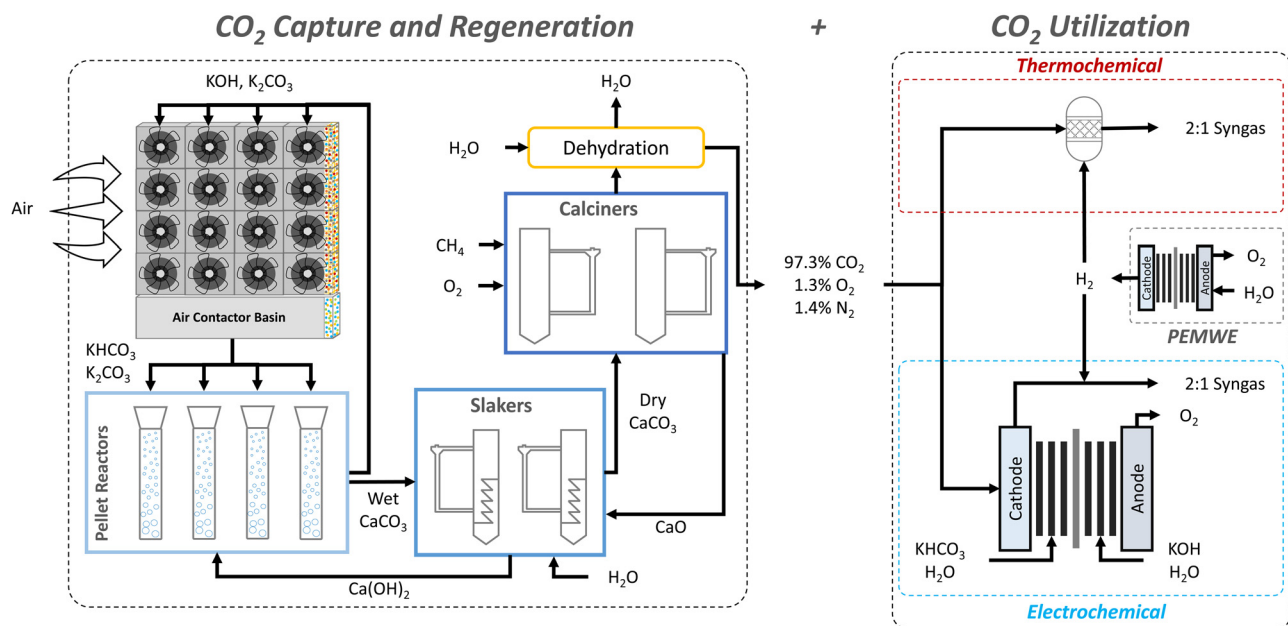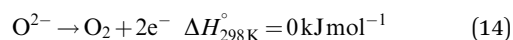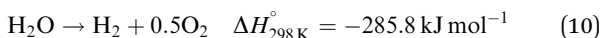
This journal is © The Royal Society of Chemistry 2023

Energy Environ. Sci., 2023, 16, 6127–6146 | 6131

Fig. 2 Process flow diagram of the investigated pathways, exhibiting the integration of hydroxide-based DACC with RWGS and with the CO₂ER. The yellow-colored monolith in the air contactors represent KOH wetting. The percentages of the CO₂ stream are based on mass.

H_2 and OH^- (eqn (11)), which crosses a membrane (either a diaphragm or an anion exchange membrane (AEM)) to the anode side where it is oxidized to produce O_2 (eqn (9)). PEMWE oxidizes water into O_2 and H^+ at the anode (eqn (12)), which then crosses a cation exchange membrane (CEM) from the anode to the cathode side, where it is reduced to H_2 (eqn (8)). In an SOEC reactor, water is reduced to H_2 and O^{2-} (eqn (13)) at high temperatures (≥ 600 °C). The oxide anion crosses a solid oxide membrane from the cathode to the anode, where it is oxidized to produce O_2 (eqn (14)). Further discussion about the three technologies can be found elsewhere.[71,72]

$$H_2O \rightarrow H_2 + 0.5O_2 \quad \Delta H^{\circ}_{298\,K} = -285.8\,kJ\,mol^{-1} \quad (10)$$

$$2H_2O + 2e^- \rightarrow H_2 + 2OH^- \quad \Delta H^{\circ}_{298\,K} = 111.7\,kJ\,mol^{-1} \quad (11)$$

$$H_2O \rightarrow 0.5O_2 + 2e^- + 2H^+ \quad \Delta H^{\circ}_{298\,K} = -285.8\,kJ\,mol^{-1} \quad (12)$$

$$H_2O + 2e^- \rightarrow H_2 + O^{2-} \quad \Delta H^{\circ}_{298\,K} = -285.8\,kJ\,mol^{-1} \quad (13)$$

$$O^{2-} \rightarrow O_2 + 2e^- \quad \Delta H^{\circ}_{298\,K} = 0\,kJ\,mol^{-1} \quad (14)$$

Out of the three methods, AWE is the most mature and stable technology with the possibility of using non-noble metals as catalysts, thus reducing the total production cost of the process.[71] PEMWE is an emerging commercial water electrolysis technology that is able to achieve higher current densities (0.6–2 A cm^{-2}) and produce high-purity hydrogen.[71] However, due to its lower TRL and use of Pt-group metals in the electrodes, it is still challenged with lower durability and higher capital costs as compared to AWE.[71,72] Nonetheless, multiple research efforts have focused on PEMWE rather than AWE due to its projected cost reductions and technological development in the upcoming decade.[72] SOEC is also projected to be a major

water electrolysis technology by 2030 and beyond because of its high energy efficiency ($\geq 95\%$), however the durability of SOEC is relatively low (500–2000 h) when compared with AWE (100 000 h) and PEMWE (10 000–50 000 h).[71] For these reasons, we choose PEMWE as the water electrolysis technology in our study and reference 4.3 kW h Nm^{-3}-H_2 as the power consumption, which is consistent with previous studies.[72,73]

2.5. Steam methane reforming (SMR)

SMR is a widely deployed process in the chemical industry for efficient H_2 production.[74,75] The process takes in a feed of CH_4 and H_2O to produce syngas at an $H_2:CO$ molar ratio of 3[39] (eqn (15)). Similar to RWGS, the referenced SMR process design uses an SMR reactor and an MEA CO_2 absorption setup to generate a concentrated H_2 stream (Fig. 1e). Note that the main purpose of the MEA CO_2 absorption setup is to clean the H_2 stream from CO_2 and other gases instead of capturing CO_2 from a point source. Consequently, the environmental impact of SMR is still concerning,[75,76] limiting its potential further usage in future carbon reduction scenarios. This has motivated its integration with CO_2 capture to produce blue hydrogen, which has been pursued by several researchers.[46,77,78] To account for this shift, we will discuss both options (i.e., emission and recycling of CO_2) in Section 5.1.[46]

$$CH_4 + H_2O \rightarrow CO + 3H_2 \quad \Delta H^{\circ}_{298\,K} = 206\,kJ\,mol^{-1} \quad (15)$$

3. Methodological approach

3.1. General method

We leveraged Aspen Plus, Aspen Energy Analyzer (AEA), and spreadsheet calculations to estimate mass and energy balances of DACC, PEMWE, and CO₂ER. To accomplish the study objectives, we built DACC and electrolysis models that consider

6132 | *Energy Environ. Sci.*, 2023, **16**, 6127–6146

This journal is © The Royal Society of Chemistry 2023

simple kinetics and thermodynamics. Then, we assessed and validated our results with literature estimates to assure consistency in the results. After that, we used our modeling results to build a techno-economic model that is able to estimate CAPEX, OPEX, and total syngas production costs. Finally, we used our techno-economic model to perform sensitivity and future scenario analyses on the emerging air-to-syngas routes. For further details on the methods used in this study, we refer the reader to Notes S1 and S2 in the ESI.†

3.2. DACC model verification

Since we are modeling the Carbon Engineering DACC process, we use Keith et al.'s pilot-plant-validated results[28] to verify our model. For the purposes of verifying our model, we focus on the first configuration of Keith et al.'s study, which utilizes natural gas and pressurizes the regenerated CO_2 to 150 bar.[28] Fig. S1 (ESI†). shows minimal differences between our and Keith et al.'s modeling results. Specifically, we look at the mass flow rates of CO_2, H_2O, O_2, and N_2 in the gas outlet of the contactor and calciner models as well as the mass flow rate of CaO in the solid outlet of the calciner model. We find the mass flow rate difference to consistently be less than 5% for all components except for O_2 in the outlet gas stream of the calciner, which shows a difference of 10%. This higher percentage is due to the different methane (and thus, oxygen) inlet flow rate to the calciner, which is lower in our model (12.75 t-CH_4 per h) than in Keith et al.'s model (13.4 t-CH_4 per h).[28] The lower methane inlet flow rate is an optimized value that sets the net heat duty of the calciner to zero, meaning that we supply the amount of heat needed by the calciner unit according to our Aspen model calculations. Moreover, for the other parts of the DACC plant, we also find consistent results with Keith et al.'s findings.[28] For instance, our model predicts that we need to make up 3.6 t-$CaCO_3$ per h to the plant, recycle 4.7 t-$CaCO_3$ per h to the pellet reactor, and recycle 22.6 t-$CaCO_3$ per h to the calciner, as shown in Tables S10 and S11 (ESI†). Keith et al. calculate these values to be 3.5, 4.5, and 21.5 t-$CaCO_3$ per h, respectively.[28] In addition, Table 1 shows the mass flow rates of a subset of key streams from Keith et al.'s study[28] and from our model, and Tables S9–S12 (ESI†) summarize all important mass balances of the air contactor, pellet reactor, calciner, and slaker for the 1 Mt-CO_2 per year plant. We find consistent results between our model and Keith et al.'s pilot-plant-based model,[28] verifying our simulation to be applicable for further scaling-up and TEA calculations.

3.3. Electrolysis model application

We apply our electrolysis model (Note S1.3. in the ESI†) to Wen and Ren et al.'s study that scaled up the CO_2 electrolyzer from

Table 1 Mass flow rates of key streams from our and Keith et al.'s models

[t per h]	Keith et al.	This work	Difference (%)
Air inlet to AC (defined)	251 000	251 000	0.00
Depleted air from AC	252 000	251 360	0.25
$CaCO_3$ inlet to calciner	300	278	7.33
CO_2 from calciner	166	164	1.20

1 cm^2 to 100 cm^2, achieving a total current density of 612 mA cm^{-2} at a cell voltage of 3.3 V, an FE_{CO} of $\geq 90\%$, and a CO_2 single-pass conversion of about 27%.[54] The exchange current density and charge transfer coefficient were taken from an earlier publication of one of the authors,[79] and their values are reported to be 8.42×10^{-4} mA cm^{-2} and 0.201, respectively. In addition, we use a 4% loss percentage of the inlet CO_2 as reported by the reference study.[54] This loss is attributed to carbonate formation and crossover from the catholyte to the anolyte, which is assumed to not release CO_2 in the anodic side, according to the findings of our reference study.[54] It is worth noting that we assume the accumulation of carbonates in the catholyte and anolyte to not influence the performance of the system. However, in our economic analysis, we consider an equivalent amount of HCl to be purchased at its market price ($84 per t-HCl80) to titrate the anolyte to the desired pH and consider purchasing some KOH at its market price ($\approx$ $450 per t-KOH81) to recover the lost amounts of K^+ to KCl.

In addition to CO_2 electrolysis, we apply the present model to PEMWE, simply calculating its mass and energy balances. We define the cathodic and anodic reactions to be the HER (eqn (8)) and water oxidation (eqn (12)), respectively. The required inputs to this model were the inlet flow rate of water and its conversions to H_2 and OH^-, which are assumed to be 100%. Eqn (S11) and (S17) (ESI†) were used to calculate the total current and the total power needed for water electrolysis, respectively. Therefore, the outputs were the product mass flow rates and the power consumption of the process.

4. Modeling results

4.1. Scaling up the DACC model

To perform our analysis, we increased the capture rate of the 1 Mt-CO_2 per year DACC plant model to match the CO_2 feed rate needed for producing 2.2 Mt-syngas per year. The modularity of our air contactor model allows us to multiply the flow rate of the captured CO_2 stream by the number of air contactors required to capture the necessary amount of CO_2 for each pathway.

The referenced RWGS model[46] requires a feed of CO_2 equal to 3.04 Mt-CO_2 per year whereas the referenced scaled-up CO_2 electrolysis system[54] requires 2.91 Mt-CO_2 per year to produce 2.26 Mt-syngas per year. For the DACC process in the DACC-PEMWE-RWGS and DACC-SMR-RWGS routes, 3350 air contactor units were used to capture 2.12 Mt-CO_2 per year, which was combined with 884 kt-CO_2 per year from the combustion of CH_4. This combination yielded 3.01 Mt-CO_2 per year, equivalent to the production of 2.26 Mt-syngas per year. The number of air contactors was reduced to 3030 units when we consider the recycling of captured CO_2 in the DACC-SMR(w/CCU)-RWGS pathway. The 3030 air contactors were able to capture 1.83 Mt-CO_2 per year and the combustion of the required methane generated 897 kt-CO_2 per year to yield 2.72 Mt-CO_2 per year. The remaining 295 kt-CO_2 per year were recycled from the PSCC step in the SMR process design, which was combined with the

This journal is © The Royal Society of Chemistry 2023

Energy Environ. Sci., 2023, **16**, 6127–6146 | **6133**

2.72 Mt-CO_2 per year to get 3.01 Mt-CO_2 per year *i.e.*, the required inlet flow rate of CO_2 to the RWGS reactor.

On the other hand, the CO_2ER pathway uses 3205 air contactor units to capture 2.03 Mt-CO_2 per year. This amount was then mixed with 847 kt-CO_2 per year from methane combustion in the calciner to yield a total capture rate of 2.88 Mt-CO_2 per year. It is worthwhile noting that the number of required air contactors at the given capture rates for both routes is only about two times that used to capture 1 Mt-CO_2 per year, simply due to the usage of CO_2 from methane combustion in the calciner.

To put these results into visual context, the number of air contactors needed for all routes is equivalent to about 0.11 km^2, or 16 FIFA-recommended football fields. It is also worth noting that these calculations assume 100% plant utilization, which is unrealistic. However, this assumption should not affect this specific analysis as the plant utilization would be applied to both the CO_2 feed requirement for RWGS/CO_2ER and to the CO_2 capture rate for DACC in later analysis.

The flow rates into subsequent units (*e.g.*, pellet reactor, slaker, and calciner) were also scaled-up by an appropriate amount to allow for processing the higher amount of captured CO_2. The amount of methane, and thus oxygen, that is fed to the calciner was scaled up such that the calciner's heat duty is equal to zero, assuring just enough heat supply for calcination. In addition, the make-up amount of $CaCO_3$ fed to the pellet reactor was scaled up to 7.4 and 7.1 t-$CaCO_3$ per h for DACC-PEMWE-RWGS and DACC-PEMWE-CO_2ER, respectively, which account for the increased losses of $CaCO_3$ at the larger scales. Tables S13–S20 (ESI†) summarize the mass flow rates of both studied routes.

Plant heat integration, as leveraged by AEA, indicates that the DACC plant requires 577.7 MW and 550.3 MW of thermal energy when integrated with RWGS and CO_2ER, respectively. This is equivalent to a natural gas input of 8.58 and 8.55 GJ per tonne of air-sourced CO_2, respectively, which is consistent with the gas input estimate from Keith and colleagues (8.81 GJ per t-CO_2).[28] The lower gas input can be attributed to the different CO_2 downstream processing. The referenced RWGS and CO_2ER processes takes in CO_2 at a temperature of 25 °C and a pressure of 1 bar. Therefore, we adjusted our model to include a cooler that reduces the outlet temperature to 25 °C, and we removed the compression stages to keep the pressure at 1 bar, resulting in a lower energy requirement than estimated by Keith and colleagues' first configuration.[28] The estimated energy consumptions of the DACC plant for each pathway will be used later in our analysis to calculate the total energy consumption of the investigated routes before estimating the total OPEX.

4.2. Electrolysis model

To keep the CO production rate constant, we estimate a required feed of 1231 t-CO_2 per h to produce 211.6 t-CO per h at a FE_{CO} of 90% and a CO_2 single-pass conversion of 27%. For this production rate, the total current is estimated to be 450 × 10^6 A. Considering a scaled-up electrolyzer area of 73 531 m^2, the current density is calculated to be 612 mA cm^{-2}, reproducing the results of our CO_2 electrolysis ref. 54. On the other hand, the anodic reaction produces 116.4 t-O_2 per h as a by-product, which

can be sold at a market price of about $100 per t-$O_2$.[82] For a cell area of 100 cm^2 per cell, as given by our CO_2 electrolysis ref. 54, an electrode area of 73 531 m^2, and a cell-to-stack ratio of 200 cells per stack, one would need about 36 766 stacks to produce the given CO amount, which is a significantly large number. Increasing the cell area from 100 cm^2 to 1 m^2 can significantly lower this number to 368, which is more reasonable and manageable than 36 766. Regardless, for this setup, we find the power consumption of the CO_2 electrolyzer to be 1484 MW. Unfortunately, low-temperature CO_2 electrolyzers to CO are not commercial yet, thus we are unable to compare this number with metrics of current commercial CO_2 electrolyzers. However, assuming a power capacity of 20 MW for a single CO_2 electrolysis module in the next 5 years, one would need 75 electrolysis modules to produce 211.6 t-CO per h.

PEM H_2O electrolyzers, on the other hand, are near the commercial stage. Indeed, Siemens' PEM water electrolyzer full module array, Silyzer 300, is planned to currently operate at a power capacity of 17.5 MW to produce 0.1–2 t-H_2 per h.[83] We estimate H_2 production *via* PEMWE in the CO_2ER pathway to be about 28.6 t-H_2 per h at an electrolyzer power consumption of 1444 MW and a current density of 2 A cm^{-2}. This calculation suggests that we would need roughly 83 Silyzer 300 module arrays to produce the required amount of renewable H_2 in the DACC-PEMWE-CO_2ER route with each system producing approximately 0.345 t-H_2 per h. We also find the electrode area to be 38 004 m^2, indicating that a Silyzer 300 module array would need a total electrode area of about 460 m^2. Similarly, for the RWGS pathway, PEMWE produces about 45.4 t-H_2 per h at an active electrode area of 60 232.9 m^2 and a power capacity of 2289 MW. These results suggest that we would need 131 Silyzer 300 module arrays with each having a total electrode area of approximately 460 m^2.

An important point is the 1.5–2.3 GW-scale water electrolyzers that we calculate as necessary to produce 2.2 Mt-syngas per year. Today, the highest capacity rating for water electrolyzers is in the range of 10–100 MW, which would be insufficient to meet renewably-driven electrolytic hydrogen production targets.[84] Thus, new water electrolysis facilities that are at the GW-scale are still needed. Indeed, the average size of new water electrolysis projects in 2030 is expected to be about 1.4 GW.[84,85] Therefore, although the scale presented here might seem significant ($\approx$1.5–2.3 GW), it is well within the projected range needed to reach electrolytic hydrogen production goals.

5. Techno-economic results

In this section, we techno-economically assess an electrochemical and a thermochemical pathway that convert air-sourced CO_2 into syngas. We include sensitivity and future scenario analyses to provide guidance on the required benchmarks for commercializing the DACC-PEMWE-CO_2ER pathway.

5.1. Technical and economic metrics

Current conventional syngas production pathways supply H_2 from fossil-based methods, such as SMR. To fairly compare

6134 | *Energy Environ. Sci.*, 2023, **16**, 6127–6146

This journal is © The Royal Society of Chemistry 2023

CO_2ER to RWGS as a CO_2 utilization technique in the presented context, we need to consider both SMR and PEMWE as H_2 production methods in the RWGS pathway. In this section, we will discuss the carbon efficiency, energy consumption and cost, and marginal energy-associated CO_2 emissions of four routes: (1) DACC-SMR-RWGS, (2) DACC-SMR(w/CCU)-RWGS, (3) DACC-PEMWE-RWGS, and (4) DACC-PEMWE-CO_2ER. It is worth mentioning that CCU in the second route refers to CO_2 capture and utilization.

5.1.1. Carbon efficiency. We define carbon efficiency to be the ratio of moles of carbon in the desired product to the moles of carbon in the carbon-based reactants (Note S4.1 in the ESI†). Fig. 3a exhibits the carbon efficiency of the full DACC-SMR-RWGS, DACC-SMR(w/CCU)-RWGS, DACC-PEMWE-RWGS, and DACC-PEMWE-CO_2ER routes, which we calculate to be 36.49%, 40.19%, 56.34%, and 20.12%, respectively. The SMR dependence on methane as a reactant to supply H_2 reduces its carbon efficiency significantly due to the fate of CO_2, which we assume

to be emitted to the atmosphere in the first route, resulting in its lower carbon efficiency when compared to DACC-PEMWE-RWGS. Recycling the CO_2 results in a higher carbon efficiency, albeit still less than DACC-PEMWE-RWGS. Furthermore, we find DACC-PEMWE-CO_2ER to have the lowest carbon efficiency, which is mainly due to the low single-pass conversion of CO_2 in the CO_2ER (27.0%) as compared to that of the RWGS process (75.6%). Kas *et al.* report that the limiting CO_2 single-pass conversion to CO may be close to 60% due to competition with homogenous reactions where CO_2 spontaneously forms (bi)carbonates when in contact with the electrolyte and does not participate in the CO_2ER.[86] Indeed, to the best of our knowledge, the highest experimental stable single-pass CO_2 conversion for gaseous alkaline CO_2ER to CO was in the range of 45–50%.[87] At a CO_2 single-pass conversion of approximately 50%, DACC-PEMWE-CO_2ER can be as carbon efficient as DACC-SMR-RWGS but will still be less carbon efficient than DACC-PEMWE-RWGS. However, if major changes in the reactor
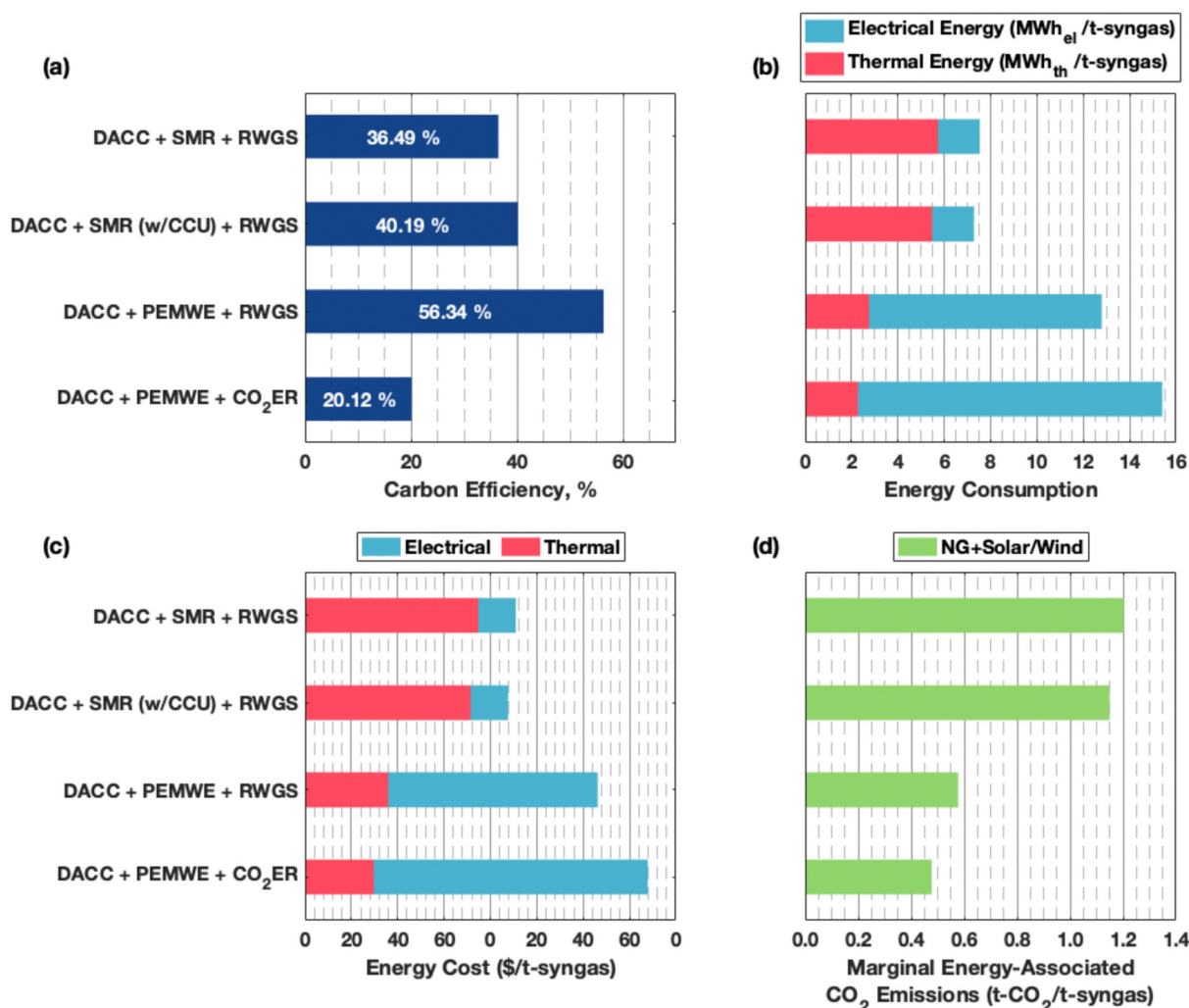
Fig. 3 (a) Carbon efficiency, (b) electrical and thermal energy consumption, (c) total energy costs, and (d) marginal CO_2 emissions associated with the energy sources for each of the three pathways. Electrical and thermal energy prices are assumed to be $45 per MW h_el and $5.03 per GJ_th, respectively. The marginal emission factor for natural gas is referenced to be 210 kg-CO_2 per MW h_th[88] whereas the marginal emission factors for solar and wind are assumed to be 0 kg-CO_2 per MW h_el.

This journal is © The Royal Society of Chemistry 2023

Energy Environ. Sci., 2023, **16**, 6127–6146 | **6135**

designs are implemented, the competition between the desired CO_2 conversion to CO and the undesired conversions to byproducts could be eliminated, resulting in the potential to break the CO_2ER carbon efficiency limit. For instance, the utilization of a bipolar membrane (BPM) in bicarbonate electrolysis allows for CO_2 to be produced in-situ, which can surpass the 60% limit imposed by the CO_2ER. Indeed, Lees *et al.* achieved a CO_2 utilization rate of about 70% in a bicarbonate flow cell reactor that utilizes a BPM as the separating membrane.[33] At this conversion, the CO_2ER and RWGS routes have very close carbon efficiencies of 52.16% and 56.34%, respectively. Improving such designs to have higher CO_2 single-pass conversions as well as increasing the CO_2 capture fraction can improve the carbon efficiency of both routes to achieve $\geq 70\%$.

5.1.2. Energy consumption and cost. Fig. 3b shows the thermal and electrical energy requirements of the four studied routes. We find electricity to dominate the total energy consumption of DACC-PEMWE-RWGS and DACC-PEMWE-CO_2ER, mainly due to the high amount of electricity required for electrolysis processes. On the other hand, DACC-SMR-RWGS and DACC-SMR(w/CCU)-RWGS mostly consume thermal energy to operate the SMR reactor at 1000 °C. Additionally, we find the electrical energy consumption of DACC-PEMWE-RWGS to be lower than that of the CO_2ER pathway due to the use of both electrolysis systems (PEMWE and CO_2ER) in the latter route as opposed to only one electrolysis system in the earlier one. On the other hand, we find a higher thermal energy consumption for the RWGS pathways compared with that of the CO_2ER pathway due to powering the RWGS reactor using additional thermal energy along with the SMR reactor in the first two routes. Translating this into energy cost demonstrates the dominance of thermal energy in the first two routes and of electricity in the latter ones (Fig. 3c). The higher electricity cost is due to the assumed high constant renewable electricity price ($45 per MW h_{el}) compared to the assumed low thermal energy price ($18 per MW h_{th}). It is worth noting that NREL's annual technology baseline (ABT) tool predicts the utility-scale solar PV levelized cost of electricity to be within the range of $12.5–52.4 per MW h for all U.S. states between the years 2024 and 2050.[89] Nevertheless, further work should be devoted to elucidating the effect of uncertain electricity prices on the economic performance of CO_2 electrolysis. For the calculations presented in this section, we refer the reader to Note S4.2. in the ESI.†

It is worthwhile noting that the considered SMR process design requires the use of an MEA CO_2 absorption setup, which is used to remove CO_2 from the H_2 product stream. Intuitively, recycling the captured CO_2 would be the best option when integrating SMR with RWGS. However, to provide a more holistic overview, we consider both the recycling and emission of the captured CO_2. The recycling of CO_2 to the RWGS reactor lowers the amount of CO_2 that needs to be captured *via* DACC, which results in a slightly lower energy consumption and cost (Fig. 3b and c). Note that almost half of the significant thermal energy consumption in the first two routes is used to operate the SMR reactor at 1000 °C and 34 bar. Therefore, only a small

difference is observed in the estimated energy consumption and cost, as can be seen in Fig. 3b and c.

5.1.3. Marginal energy-associated CO_2 emissions. The energy-associated CO_2 emissions can be estimated using a marginal emission factor, which is defined as the change in CO_2 emissions due to the additional generation/consumption of a unit of energy.[88] We set the marginal emission factor of natural gas, solar, and wind to be 210, 0, and 0 kg-CO_2 per MW h, as reported by Huber and colleagues.[88] Fig. 3d shows this metric for the four studied pathways. We find that recycling the captured CO_2 from SMR to RWGS results in slightly lower marginal energy-associated CO_2 emissions. Remember that the main difference in energy consumption for the two SMR pathways is the amount of CO_2 produced *via* DACC. Thus, the emission difference is due to the lower thermal energy usage of the DACC plant. Furthermore, we observe a trade-off between energy consumption/cost and marginal energy-associated CO_2 emissions. In other words, although the CO_2 electrolysis pathway consumes more energy, its marginal energy-associated CO_2 emissions are estimated to be lower than those from the conventional RWGS pathways. The scale of this trade-off should help decision makers as to whether the emerging pathway is a competitive alternative.

Currently, DACC-PEMWE-CO_2ER might not be the most economic option to replace the conventional RWGS pathways. We estimate that it would require an additional $1146 million per year for a CO_2 emission reduction of 1.49 Mt-CO_2 per year with DACC-PEMWE-CO_2ER replacing DACC-SMR-RWGS. This number translates to a CO_2 avoidance cost of $769 per t-$CO_2$-avoided at electricity and natural gas prices of $45 per MW h and $5.03 per GJ, respectively. Through similar calculation and using the same assumptions for the electricity and natural gas prices, we estimate the replacement of DACC-SMR-RWGS by DACC-PEMWE-RWGS to require a CO_2 avoidance cost of $576 per t-$CO_2$-avoided. Reducing the electricity price by $5 per MW h reduces the two CO_2 avoidance costs of DACC-PEMWE-CO_2ER and DACC-PEMWE-RWGS by $95 per t-$CO_2$-avoided and $72 per t-$CO_2$-avoided, respectively. Indeed, an electricity price of $15 per MW h results in a CO_2 avoidance cost of $\leq \$200$ per t-CO_2-avoided. Therefore, increasing CO_2 taxes while reducing electricity prices might enable SMR replacement with PEMWE when using RWGS for syngas production. Additionally, it can allow CO_2ER to compete with RWGS in today's scenario, where SMR is conventionally used as a H_2 production method. Nonetheless, performing sensitivity and future scenario analyses on relevant parameters and investigating future scenarios should elucidate how CO_2ER may compete with RWGS when integrated with hydroxide-based DACC and PEMWE. Thus, we pivot away from DACC-SMR-RWGS and DACC-SMR(w/CCU)-RWGS hereinafter.

5.1.4. Capital and operational cost estimation. Estimating the capital and operational costs requires equipment sizing and cost information, which can be obtained from historical data and process modeling results. Table 2 summarizes the major equipment and their sizing parameters that are used to estimate their installed equipment costs (IECs) for both DACC-PEMWE-RWGS and DACC-PEMWE-CO_2ER. In this work, we

6136 | *Energy Environ. Sci.,* 2023, **16**, 6127–6146

This journal is © The Royal Society of Chemistry 2023

Table 2 Equipment information, sizing, conditions, and installed 2021 costs for a syngas production rate of 23 100 kmol-syngas per h (2.26 Mt-syngas per year) at an H_2 : CO ratio of 2 for DACC-PEMWE-RWGS and DACC-PEMWE-CO_2ER

Equipment	Sizing parameter and notes	Installed cost ($)
DACC – PEMWE – RWGS pathway		
Direct air CO_2 capture plant		
Air contactor	Fans, centrifugal[a]	146.43×10^6
	$\dot{V} = 1.34 \times 10^5$ m^3 h^{-1}; 3350 units	
	Structured PVC packing[b]	636.24×10^6
	Volume = 175 m^3; 3350 packings	
	Single-stage centrifugal pump[c]	3.10×10^6
	$\dot{V} = 134.78$ L s^{-1}; 21 pumps	
Pellet reactor	Forced circulation crystallizer[a]	144.05×10^6
	Solids capacity = 1.78 kg s^{-1}; 101 units	
Slaker	Fluidized bed dryer[a]	8.27×10^6
	Fluidization velocity = 1 m s^{-1}; 25 units	
Calciner	Cylindrical furnace[c]	125.44×10^6
	Duty = 4.60 MW; 84 units	
Air separation unit (ASU)	Referenced from Keith et al.[28]	148.60×10^6
Heat exchange network (HEN)	Generated using AEA, estimated using Towler and Sinnot[90]	804.33×10^6
Total installed costs		*2.02×10^9*
Proton exchange membrane water electrolysis		
H_2O PEM electrolyzer[d]	$C_{ref} = \$460$ kW^{-1}h^{-1}; $j_{H_2} = 2$A cm^{-2}; $V_{cell} = 1.9$ V	1.65×10^9
Total installed costs		*1.65×10^9*
Reverse water gas shift plant[46]		
Total installed costs[e]		*139.93×10^6*
DACC – PEMWE – CO_2ER pathway		
Direct air CO_2 capture plant		
Air contactor	Fans, centrifugal[a]	140.09×10^6
	$\dot{V} = 133\,668.2$ m^3 h^{-1}; 3205 units	
	Structured PVC packing[b]	608.70×10^6
	Volume = 175 m^3; 3205 packings	
	Single-stage centrifugal pump[c]	2.96×10^6
	$\dot{V} = 134.78$ L s^{-1}; 20 pumps	
Pellet reactor	Forced circulation crystallizer[a]	137.39×10^6
	Solids capacity = 1.79 kg s^{-1}; 96 units	
Slaker	Fluidized bed dryer[a]	7.94×10^6
	Fluidization velocity = 1 m s^{-1}; 24 units	
Calciner	Cylindrical furnace[c]	119.51×10^6
	Duty = 4.60 MW; 80 units	
Air separation unit (ASU)	Referenced from Keith et al.[28]	142.17×10^6
Heat exchange network (HEN)	Generated using AEA, estimated using Towler and Sinnot;[90]	756.22×10^6
Total installed costs		*1.92×10^9*
Proton exchange membrane electrolysis cell		
H_2O PEM electrolyzer[d]	$C_{ref} = \$460$ kW^{-1}h^{-1}; $j_{H_2} = 2A$ cm^{-2}; $V_{cell} = 1.9$ V	1.04×10^9
Total installed costs		*1.04×10^9*
CO_2 electrolysis		
CO_2 electrolyzer[d]	$C_{ref} = \$460$ kW^{-1}h^{-1}; $j_{CO,actual} = 0.55\,A$ cm^{-2}; $V_{cell} = 3.5$ V	2.20×10^9
Pressure swing adsorption	$\dot{V}_{ref} = 1000$ m^3 h^{-1}; $C_{ref} = \$1.989 \times 10^6$; scaling factor = 0.70	
	$\dot{V}_{Cathode} = 312, 335.26$ m^3 h^{-1}	323.08×10^6
	$\dot{V}_{Anode} = 297, 124.68$ m^3 h^{-1}	311.98×10^6
Total installed costs		*2.84×10^9*

[a] The instrumentation estimate and parameters were taken from Woods when estimating the IEC.[91]   [b] An installation factor of 3.2 was used for the PVC packing, as calculated by McQueen et al. from Keith and colleagues' given data.[17,28]   [c] Parameters were taken from Towler and Sinnot[90] when estimating the IEC.   [d] We refer to the H_2A production model[53] for both H_2O and CO_2 electrolyzer cost estimations.   [e] The full cost breakdown of the RWGS plant can be found in Rezaei and Dzuryk's work.[46]

consider the total IECs to be equivalent to the total inside battery limit (ISBL) costs, which include both direct (*e.g.*, major process equipment costs) and indirect (*e.g.*, construction costs and insurance) field costs. Additionally, we consider a plant production rate of 2.26 Mt-syngas per year for both routes and an H_2 : CO ratio of 2 : 1, and we extrapolate the installed costs to the year 2021. As mentioned above, we no longer consider the

DACC-SMR-RWGS or DACC-SMR(w/CCU)-RWGS hereinafter as we are mostly interested in assessing the emerging, more-environmental routes.

Fig. 4 shows the ISBL (*i.e.*, capital) cost breakdown structure of each pathway, considering a plant utilization of 90%. We find the air contactors, DACC heat exchanger networks (HENs), and electrolyzers to be the three largest contributors to the
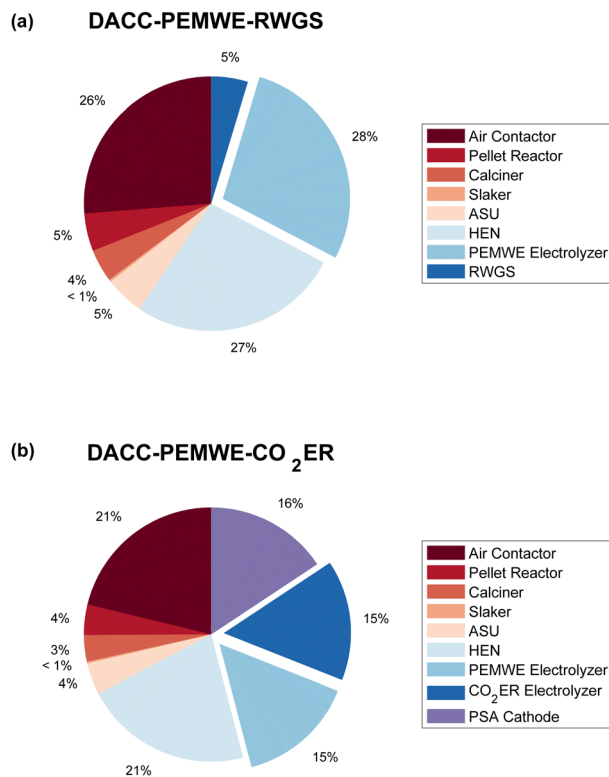
This journal is © The Royal Society of Chemistry 2023

Energy Environ. Sci., 2023, **16**, 6127–6146 | **6137**

(a) DACC-PEMWE-RWGS

Legend:
- Air Contactor
- Pellet Reactor
- Calciner
- Slaker
- ASU
- HEN
- PEMWE Electrolyzer
- RWGS

(b) DACC-PEMWE-CO$_2$ER

Legend:
- Air Contactor
- Pellet Reactor
- Calciner
- Slaker
- ASU
- HEN
- PEMWE Electrolyzer
- CO$_2$ER Electrolyzer
- PSA Cathode

Fig. 4 ISBL cost breakdown structure of (a) DACC–PEMWE–RWGS and (b) DACC–PEMWE–CO$_2$ER, showing the percentages of cost components. Exploded: electrolyzers.

(a) DACC-PEMWE-RWGS

Legend:
- CAPEX (DACC)
- CAPEX (PEMWE)
- CAPEX (RWGS)
- vOPEX (DACC)
- vOPEX (PEMWE)
- vOPEX (RWGS)
- Electricity Costs
- fOPEX (DACC)
- fOPEX (PEMWE)
- fOPEX (RWGS)

(b) DACC-PEMWE-CO$_2$ER

Legend:
- CAPEX (DACC)
- CAPEX (PEMWE)
- CAPEX (CO$_2$ER)
- vOPEX (DACC)
- vOPEX (PEMWE)
- vOPEX (CO$_2$ER)
- Electricity Costs
- fOPEX (DACC)
- fOPEX (PEMWE)
- fOPEX (CO$_2$ER)

Fig. 5 The percentages of CAPEX, variable OPEX, electricity costs, and fixed OPEX of each technology for (a) DACC–PEMWE–RWGS and (b) DACC–PEMWE–CO$_2$ER pathways. Exploded: CAPEX fractions. Non-exploded: OPEX fractions. Note that the vOPEX percentage excludes electricity costs, which has its own contribution.

capital cost of both routes. Notably, the capital costs of electrolyzers takes up the majority of the total ISBL costs of both routes with shares of 28% and 30% in DACC-PEMWE-RWGS and DACC-PEMWE-CO$_2$ER, respectively. HENs and air contactors are ranked second with significant shares of 26–27% and 21% in the RWGS and CO$_2$ER pathways, respectively. This result suggests that improving and optimizing the electrolyzer and DACC process designs is critical for reducing the total capital cost.

Furthermore, particular attention should be paid to the downstream PSA separation step in the DACC-PEMWE-CO$_2$ER pathway. We find the CAPEX of downstream PSA separation and the CO$_2$ electrolyzer to be of a similar magnitude, demonstrating the importance of maximizing the CO$_2$ single-pass conversion. This finding supports some recent efforts that investigated the importance of downstream separation of CO$_2$ in the CO$_2$ER.[92,93] However, it is worth noting that a trade-off might exist between CO$_2$ER performance and downstream separation costs, encouraging further studies of downstream separation on the CO$_2$ER to CO, similar to a recent effort that investigated this trade-off for CO$_2$ER to ethylene.[94]

Fig. 5 exhibits the breakdown of the total syngas cost (in %) into CAPEX, variable OPEX, and fixed OPEX of each process included here – *i.e.*, DACC, PEMWE, RWGS, and CO$_2$ER–as well as the electricity cost of the whole pathways. Note that electricity costs are excluded from the variable OPEX amounts and are included as a separate component in Fig. 5. The OPEX also
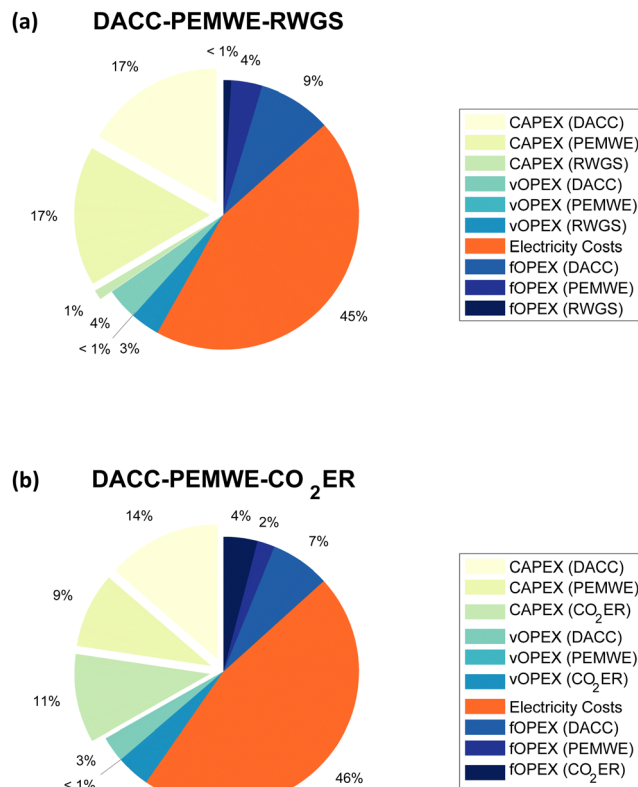
considers a plant utilization of 90%. We find both the RWGS and CO$_2$ER pathways to be OPEX-intensive with OPEX shares of about 66% (sum of all OPEX components) of the total syngas cost, which is dominated by electricity costs in both routes. This result highlights the essential role that electricity prices will play in reducing the total syngas production costs of air-to-syngas routes. However, wholesale electricity prices vary in time, and the least cost renewable energy sources (wind and solar PV) have both variable and uncertain outputs. Thus, future studies should explore and assess the integration of such pathways with solar and wind power plants as well as with future electricity grids that includes a significant portion of renewable sources in their mixtures.

Moreover, any further energy efficiency improvements would reduce the electricity cost contribution significantly, especially for the second route because the CO$_2$ER is assumed to have an energy efficiency of less than 45%. In the present scenario, the total syngas production cost *via* the RWGS and CO$_2$ER pathways are $1.09 per kg-syngas and $1.25 per kg-syngas, respectively. Increasing the CO$_2$ER energy efficiency to 81%, equivalent to operating at 1.82 V, can reduce the total syngas cost of DACC-PEMWE-CO$_2$ER by 13.1%, enabling CO$_2$ER to economically compete with RWGS in the studied configuration at the considered CO$_2$ER performance (*i.e.*, total current

6138 | *Energy Environ. Sci.*, 2023, **16**, 6127–6146

This journal is © The Royal Society of Chemistry 2023

density = 612 mA cm^{-2}, CO_2 single-pass conversion = 27%, FE_{CO} = 90%, cell voltage = 3.30 V).

Furthermore, the contribution of DACC in the total production cost of syngas is of interest to the DACC community. Our TEA estimates the CO_2 capture cost of hydroxide-based DACC to be approximately $220 per t-$CO_2$. This cost accounts for 29.7% and 24.2% of the total production cost of syngas for DACC-PEMWE-RWGS and DACC-PEMWE-CO_2ER, as shown in Fig. 5.

5.2. Sensitivity analysis

To understand the effect of different technical and economic parameters on the total syngas production cost, we performed sensitivity analysis. We kept the Butler–Volmer relationship implemented, meaning that we assumed no improvement in the electrolyzer design here. Consequently, the effect of current density and cell voltage on the total syngas cost will be embedded in the variations of the CO_2 electrolyzer area and FE_{CO}. For further information on this point, we refer the reader to Note S1.3 in the ESI.† In the Future scenarios section, however, we will consider electrolyzer design improvements.

Table 3 summarizes the three considered cases for the sensitivity analysis of both routes. For both pathways, we consider PEM H_2O electrolyzer CAPEX, electricity prices, H_2 production costs, CO_2 capture costs, and natural gas prices. In the CO_2ER pathway, we additionally consider CO_2 electrolyzer CAPEX, CO_2 electrolyzer area, CO_2 single-pass conversion, and FE_{CO}. We focus this sensitivity analysis mostly on improving CO_2ER as a CO_2 utilization method since it is a less mature technology than RWGS. Note that the conservative and future cases represent ±33% of the baseline case. However, for FE_{CO}, 100% FE_{CO} is assumed in the future case.

The tornado plots in Fig. 6 show that the total syngas production cost (TPC$_{syngas}$) of DACC-PEMWE-RWGS ($1.09 per kg-syngas) is lower than that of DACC-PEMWE-CO_2ER ($1.25 per kg-syngas), which should be expected since RWGS is more technologically mature than CO_2 electrolysis. Furthermore, we find the H_2 production cost and the electricity price to be the main drivers of both routes. However, the TPC$_{syngas}$ of the first pathway is more sensitive to H_2 production costs whereas the
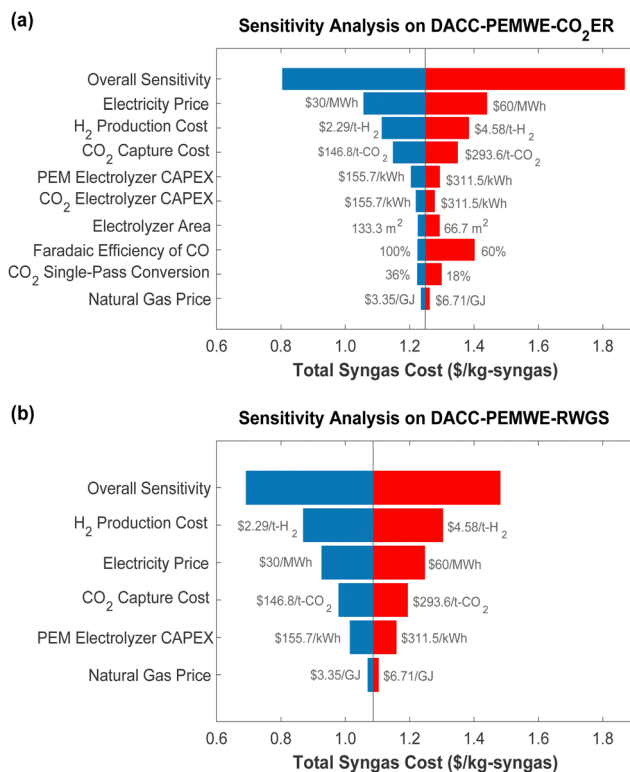
Fig. 6 Sensitivity analysis on technical and economic metrics for (a) DACC-PEMWE-RWGS and (b) DACC-PEMWE-CO_2ER.

TPC$_{syngas}$ of the second pathway is more sensitive to electricity prices. This is most likely due to the higher required amount of H_2 for RWGS than for CO_2ER and due to the greater electricity dependence of the CO_2ER pathway. Regardless of the order, it is worth noting that the H_2 production costs also heavily depend on electricity prices since we are assuming H_2 production *via* electrolysis. Thus, it is safe to say that the electricity price is the main cost driver of the presented pathways.

Moreover, we find a significant sensitivity of the TPC$_{syngas}$ of both routes towards the CO_2 capture cost, indicating that DACC process improvements are still needed to enable commercialization of an economic air-to-syngas process. As shown in Fig. 4, the air

Table 3 Sensitivity analysis parameters and cases for both emerging routes. Grey results are outputs of varying a parent parameter (*i.e.*, Electrolyzer Area or FE_{CO})

Parameter	DACC-PEMWE-RWGS			DACC-PEMWE-CO_2ER		
	Conservative	Baseline	Future	Conservative	Baseline	Future
Electricity price ($ per MW h)	60 (+33%)	45	30 (−33%)	60 (+33%)	45	30 (−33%)
H_2 production cost ($ per kgH$_2$)	4.57 (+33%)	3.43	2.29 (−33%)	4.57 (+33%)	3.43	2.29 (−33%)
CO_2 capture cost ($ per t-CO_2)	295.5 (+33%)	221.6	147.8 (−33%)	293.7 (+33%)	220.2	146.8 (−33%)
PEM electrolyzer CAPEX ($ per kW)	311.5 (+33%)	233.6	155.7 (−33%)	311.5 (+33%)	233.6	155.7 (−33%)
CO_2 electrolyzer CAPEX ($ per kW)	—	—	—	311.5 (+33%)	233.6	155.7 (−33%)
Electrolyzer area (cm^2)	—	—	—	66.7 (+33%)	100	133.3 (−33%)
Cell voltage (V)	—	—	—	3.8	3.3	3.1
Current density (mA cm^{-2})	—	—	—	918.0	612.0	459.0
FE_{CO}	—	—	—	60% (−33%)	90%	100% (+11%)
Cell voltage (V)	—	—	—	3.8	3.3	3.2
Current density (mA cm^{-2})	—	—	—	918.0	612.0	550.8
CO_2 single-pass conversion	—	—	—	18% (−33%)	27%	36% (+33%)
Natural gas price ($ per GJ)	6.71 (+33%)	5.03	3.35 (−33%)	6.71 (+33%)	5.03	3.35 (−33%)

This journal is © The Royal Society of Chemistry 2023

Energy Environ. Sci., 2023, **16**, 6127–6146 | **6139**

contactor and HENs contribute significantly to the capital cost of both routes. Thus, improving the air contactor and plant designs is key to reducing the TPC_{syngas} of the presented pathways. These results suggest that reducing renewable electricity prices (and thus, H_2 production costs) and CO_2 capture costs might be the most relevant economic targets for an air-to-syngas process in the meantime.

The sensitivity analysis also considered technical parameters of CO_2 electrolysis. However, improving these parameters can lower the syngas cost by up to 2% per parameter. On the other hand, worsening the technical parameters can increase the syngas cost by more than 2%, which is due to nonlinearity. Indeed, we find that lowering the FE_{CO} to 60%, reducing the reference electrolyzer area to 66.7 cm2, and decreasing the CO_2 single-pass conversion to 18% result in increasing the cost of syngas by about 20% to a value of $1.50 per t-syngas. Thus, maintaining the performance of CO_2ER as it scales up is essential to realizing an economic air-to-syngas process.

To complete the picture, we also considered the capital cost of H_2O and CO_2 electrolyzers as well as the natural gas price. We find these three parameters do not affect the cost of syngas significantly. However, their cumulative optimistic assumptions can help improve the pathway economics by up to 8.2% and 7.1% for the RWGS and CO_2ER pathways, respectively.

5.3. Future scenario analysis

The potential for integration of CO_2ER or RWGS with DACC in the presented configurations depends on several factors including the technological maturity of CO_2 electrolysis, CO_2 taxes and tax credits, CO_2 capture costs, H_2 production costs, natural gas prices, and renewable electricity prices. If the proposed integrated designs are to be realized for net-zero targets, all of the considered technologies must be developed and deployed at industrial scales by 2050. Note that our assumptions (*e.g.*, electricity price and plant scale) are based on realizing net-zero emissions by 2050.[7,17,89] In this section, we consider the implications of an improved CO_2 electrolysis process with an FE_{CO} of 90%, a CO_2 single-pass conversion of 54%, and a total current density of 1.5 A cm^{-2}. Table 4 summarizes the assumptions made for the future scenario analysis.

To account for process design improvements, we considered four low cell voltages of 2.50, 2.25, 2.00, and 1.75 V. To the best

of our knowledge, the lowest reported cell voltage that operates at current densities of ≥ 200 mA cm^{-2} for gaseous CO_2 electrolysis is about 2.00 V.[95] We chose the lowest cell voltage to be 1.75 V, representing an extremely optimistic case in the event of a significant improvement in the energy efficiency of CO_2 electrolysis. Furthermore, we assume the CO_2 capture cost to be $100 per t-$CO_2$ for all future scenarios, which is consistent with the carbon negative shot target, set by the U.S. department of energy (DOE). Finally, we use a 2050-projected industrial natural gas price of $4.52 per GJ, as given in the 2023 U.S. energy information administration (EIA) annual energy outlook report.[96]

Fig. 7 shows the total syngas and H_2 production costs under variable electricity prices and CO_2 tax and tax credits at four different cell voltages. We find that reducing the cell voltage to 2.50 V is insufficient for DACC-PEMWE-CO_2ER to compete with DACC-PEMWE-RWGS economically. At a cell voltage of 2.25 V, however, the competition begins to appear at high electricity prices ($\geq$$65 per MW h). As the cell voltage reduces to 2.00 V and 1.75 V, one can observe a more pronounced economic potential for the CO_2ER as compared to RWGS in the studied configurations. This result suggests that improving the energy efficiency of the CO_2ER to above 70% will still be key to CO_2 electrolysis commercialization even at high current densities (≈ 1.5 A cm^{-2}), high FE_{CO} ($\approx 90\%$), and high CO_2 single-pass conversions ($\approx 54\%$) due to the competition with RWGS. Thus, achieving cell voltages of about 2.00 V (energy efficiency = 73.5%) is a prerequisite to realizing an economically feasible DACC-PEMWE-CO_2ER process, consistent with recommendations made by other researchers.[61,97]

Furthermore, the comparison of these emerging syngas production pathways with traditional ones is essential to understanding their market potential. The approximate U.S. syngas price is calculated to be $0.65 per kg-syngas, which is represented by the dotted line in Fig. 7. This price was calculated from the prices of CO and H_2 in the U.S. that were reported in the 2021 IHS Markit process economics program (PEP) yearbook.[98] It is worthwhile noting that this price is consistent with estimates used in the literature, which range from $0.2 per kg-syngas to $0.74 per kg-syngas.[38,46,52] We find DACC-PEMWE-CO_2ER to compete economically with conventional routes when electricity prices are $\leq$$24 per MW h, $\leq$$26 per MW h, $\leq$$28 per MW h, and $\leq$$30 per MW h for the cell voltages of 2.50, 2.25, 2.00, and 1.75 V, respectively, and at a CO_2 tax and tax credit of $100 per t-$CO_2$. If the CO_2 tax and tax credits increase to $300 per t-$CO_2$, the target electricity prices would be $\leq$$38 per MW h, $\leq$$40 per MW h, $\leq$$42 per MW h, and $\leq$$45 per MW h, respectively. On the other hand, if no CO_2 tax and tax credit were considered, the target electricity prices drop to $\leq$$18 per MW h, $\leq$$19 per MW h, $\leq$$21 per MW h, and $\leq$$23 per MW h (Fig. S2, ESI†). This finding highlights the important role of CO_2 taxes and tax credits in commercializing renewably-driven air-to-chemical processes. To put this into context, the recent changes made by the U.S. inflation reduction act (IRA) to section 45Q for CO_2 capture credits increased the tax credit for producing chemical from air-

Table 4 Design specifications of future scenarios

Parameter	Value/range
Electricity price	$5–65 per MW h
CO_2 tax	$100–300 per t-$CO_2$
CO_2 tax credit	$100–300 per t-$CO_2$
Natural gas price	$4.52 per GJ
CO_2 capture cost	$100 per t-$CO_2$
CO_2 electrolyzer CAPEX	$233.61 per kW
H_2O electrolyzer CAPEX	$233.61 per kW
Current density (CO_2ER)	1.5 A cm^{-2}
Cell voltage (CO_2ER)	2.50 V/2.25 V/2.00 V/1.75 V
CO_2 single-pass conversion	54%
CO faradaic efficiency	90%

6140 | *Energy Environ. Sci.*, 2023, **16**, 6127–6146

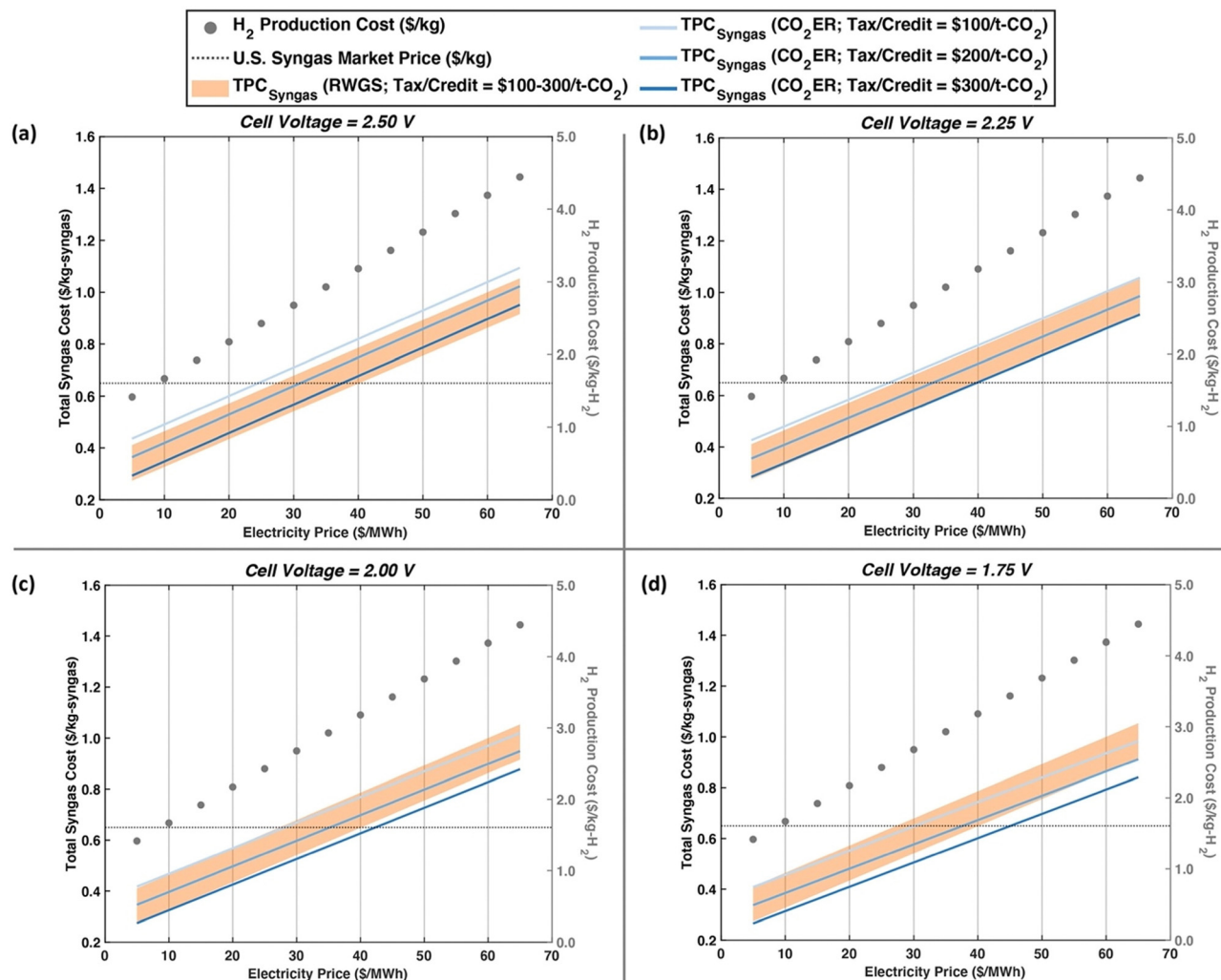This journal is © The Royal Society of Chemistry 2023

Fig. 7 Future scenarios of the two studied routes considering a range of electricity prices ($5–65 per MW h) and three CO_2 tax and tax credit assumptions ($100 per t-$CO_2$, $200 per t-$CO_2$, and $300 per t-$CO_2$). The four cases are considering improved CO_2ER cell voltages of (a) 2.50 V, (b) 2.25 V, (c) 2.00 V, and (d) 1.75 V. Note that an overall improved CO_2ER performance and a CO_2 capture cost of $100 per t-$CO_2$ are considered here. The circular markers represent H_2 production cost. The dotted line represents the U.S. syngas cost based on 2021 IHS Markit PEP yearbook price data.[95] The shaded orange region represents the TPC$_{syngas}$ of DACC-PEMWE-RWGS and the blue lines represent the TPC$_{syngas}$ of DACC-PEMWE-CO_2ER with each shade representing a CO_2 tax and tax credit (light: $100 per t-$CO_2$, medium: $200 per t-$CO_2$, dark: $300 per t-$CO_2$).

sourced CO_2 to $130 per t-$CO_2$, requiring electricity prices to be $\leq$$26 per MW h, $\leq$$28 per MW h, $\leq$$30 per MW h, and $\leq$$32 per MW h for the 2.50, 2.25, 2.00, and 1.75 V scenarios, respectively (Fig. S3, ESI†). Note that electricity price targets for the different future scenarios fall within or above projected renewable electricity prices in 2050 ($12.5–31.6 per MW h[89]), opening the door for an economically feasible air-to-syngas route that leverages improved low-temperature CO_2 electrolysis, which can be driven by intermittent renewable power sources.

6. Implications of the study

6.1. Integration with renewable energy

The significant 45–46% contribution of electricity to the total syngas production cost entails optimizing system design,

process integration, and process operation to minimize electricity costs for the cost-competitiveness of the emerging air-to-syngas production pathways. To this end, integration with variable renewable power sources (e.g., wind and solar photovoltaic) and electricity markets should be considered in more detail. For example, co-location with variable renewable power sources could be allowed by flexible air-to-syngas processes, which could reduce the need for electrical energy storage.[25,99] In addition, integrating with renewable grid-electricity could reduce the electricity cost, benefiting from dynamic electricity prices.[100] However, depending on the technology, variable operation of electrolysis processes could reduce the lifetime of the electrolyzers (e.g., lead to degradation of components), which could increase the replacement costs.[25] Additionally, the associated carbon footprint of grid-electricity could limit the environmental benefits of emerging syngas production

This journal is © The Royal Society of Chemistry 2023

Energy Environ. Sci., 2023, **16**, 6127–6146 | **6141**

pathways and their integration with electricity markets. Therefore, the value of flexibility of alternative syngas production pathways in view of variable renewable power sources and electricity markets needs to be addressed in future efforts.

Moreover, powering electrolyzers solely with dedicated variable renewable energy resources will likely require the plant capacity factor to be in the range of 21–79%, depending on the renewable power source and its availability.[25] As a result, a higher capital cost per mass of product would be expected, which would increase the total production cost of syngas. However, it is worth noting that there is a trade-off between electricity and capital costs. For example, for grid-driven electrolysis, the optimal capacity factor varies from 40% to 95% for water electrolyzers, depending on how dynamic electricity prices or rates are.[100] Thus, further research on the trade-offs between the economics and carbon emissions of grid-integrated electricity and dedicated renewable generation is required.

6.2. Social considerations

Our exploration of an air-to-syngas process here suggests several technical and economic improvements such as enhancing the electrolyzer energy efficiency as well as the reduction of green H_2 production cost and air-sourced CO_2 capture cost, which influence the total production cost of syngas significantly. However, it is critical that we explore these emerging routes from a social point-of-view to understand some of their potential social and worldwide impacts.

An environmentally attractive feature of the emerging air-to-syngas pathways studied here is the displacement of existing syngas production methods. Our results indicate that the energy-related carbon footprint of syngas production *via* DACC-SMR-RWGS, which is the closest pathway to traditional syngas production, is 1.32 kg-CO_2 per kg-syngas, summing up to be about 2.99 Mt-CO_2 per year in the studied scale (*i.e.*, 2.26 Mt-syngas per year). Deploying DACC-PEMWE-CO_2ER could reduce syngas-related CO_2 emissions by at least 50% (Fig. 3d). It is worthwhile noting that this comparison considers the SMR-RWGS pathway to source its carbon from air, which is not the case in currently commercialized syngas production plants. In addition, since we are dealing with emerging technologies and integrated pathways, the best siting location of these processes is yet to be determined. Indeed, existing renewable energy sources, including wind and solar, and available nonarable lands can provide advantages to one location over another. Thus, the shift to a defossilized syngas production method can create employment opportunities in historically underserved communities and countries, resulting in a contribution to several of the seventeen United Nations' sustainable development goals (SDGs) including climate action, decent work and economic growth, and industry, innovation, and infrastructure.[101] However, it is worthwhile noting that producing electrolytic H_2, a key reactant and product in air-to-syngas pathways, requires continuous access to water, which is a limited resource in several regions of the world.[102] In fact, our model predicts that 8.9 L of water is needed to produce 1 kg

of H_2 *via* PEMWE, equivalent to about 9740 m^3 of water at the scale given in this study. This is also equivalent to the daily consumption of 295 088 people, depending on their geographical location and water consumption.[103] For instance, in Rwanda, it is equal to the daily water consumption of 190 939 individuals whereas in the U.S., it is equal to the daily water consumption of merely 2597 persons. The huge difference in these numbers is mainly due to the fact that the water consumption per capita in the U.S. is higher than that in Rwanda. Therefore, careful siting of these plants must be seriously considered to avoid competition with basic human rights.

The given social considerations are by no means comprehensive. Further assessment studies that consider the social implications of emerging renewable or sustainable routes should still be pursued to build an understanding of human rights challenges as we pursue a sustainable worldwide economy.

7. Conclusions

In this effort, we developed and verified a DACC model in Aspen Plus based on Carbon Engineering's design. We also developed an electrolysis model to be applied to CO_2 and water electrolysis. In addition, we referenced a RWGS model and an SMR model from the literature to fill the gap in our integrated assessment. We used these models to assess DACC-SMR-RWGS, DACC-PEMWE-RWGS, and DACC-PEMWE-CO_2ER pathways in terms of carbon efficiency, energy consumption, energy cost, and marginal energy-associated CO_2 emissions. Finally, we performed a full techno-economic assessment of DACC-PEMWE-RWGS and DACC-PEMWE-CO_2ER to understand the effects of technical and economic parameters as well as process design improvements on the total syngas production cost.

Our findings demonstrate a trade-off between energy consumption/cost and marginal energy-associated CO_2 emissions, with higher energy consumption and costs for DACC-PEMWE-CO_2ER and higher emissions for DACC-SMR-RWGS and DACC-PEMWE-RWGS. We find that displacement of current syngas production methods with CO_2 electrolysis can be achieved at renewable electricity prices of $\leq\$15$ per MW h and CO_2 avoidance costs of \$200 per t-CO_2. In addition, our techno-economic assessment demonstrates that reducing the cost of DACC and the price of electricity are the key drivers to enable a commercial air-to-syngas process. Interestingly, we find the technical parameters of the CO_2ER (single-pass conversion, FE$_{CO}$, electrolyzer area, *etc.*) to have a minor influence on the total syngas cost, compared to the rest of the process. Finally, our future scenario analysis shows that an improved CO_2ER process (FE$_{CO}$ = 90%, CO_2 single-pass conversion = 54%, CO current density = 1.5 A cm^{-2}, V_{cell} = 2.00 V) is able to compete economically with RWGS in the studied configuration when the electricity price is $\leq\$28$–42 per MW h, given a CO_2 capture cost of \$100 per t-CO_2, CO_2 tax and tax credit of at least \$100 per t-CO_2, a natural gas price of \$4.52 per GJ, and a CO_2 electrolyzer CAPEX of \$233.61 per kW. Higher CO_2 taxes and/or tax credits allow more flexibility in electricity prices, which can speed up

6142 | *Energy Environ. Sci.*, 2023, **16**, 6127–6146

This journal is © The Royal Society of Chemistry 2023

commercialization of a carbon-neutral air-to-syngas process using hydroxide-based DACC, PEMWE, and CO_2 electrolysis technologies.

At the current technological stage, defossilized air-to-syngas pathways would benefit the most from reduced electricity prices, which would in turn help reduce the H_2 production cost *via* electrolysis, and from more energy and cost efficient DACC process designs. Achieving the U.S. DOE carbon negative shot target of $100 per t-$CO_2$, reducing renewable electricity prices to $20–40 per MW h, and increasing the CO_2 tax and tax credits to $\geq$$100 per t-CO_2 are the three most influential goals to realizing a commercial defossilized air-to-syngas process. In addition, flexibility in integration with variable renewable power systems is yet to be explored, which can clarify the potential of such pathways to be powered by renewables. In parallel to achieving these techno-economic goals, serious considerations of social impacts of such emerging pathways should be discussed, providing holistic assessments that would help decision-makers and the public in selecting the most suitable technologies for deployment.

Author contributions

Conceptualization, H. M. A., A. S. T., W. A. S., and B. M. H.; methodology, H. M. A. and A. S. T.; validation, H. M. A.; investigation, H. M. A.; writing – original draft, H. M. A. and O. J. G.; writing – review & editing, H. M. A., O. J. G., W. A. S., B. M. H., and A. S. T.; visualization, H. M. A.; supervision, W. A. S., B. M. H., and A. S. T.

Conflicts of interest

There are no conflicts to declare.

Acknowledgements

References

1 *International Energy Agency. CO2 Emissions, 2022*, IEA Publications, Paris, 2023, p. 17, Available from: **https://iea.blob.core.windows.net/assets/3c8fa115-35c4-4474-b237-1b00424c8844/CO2Emissionsin2022.pdf**.

2 IPCC, *Special Report: Global Warming of 1.5 °C: Summary for Policymakers*, Cambridge University Press, UK and New York, NY, USA, 1st edn, 2018, pp. 3–24. Available from: **https://www.cambridge.org/core/product/identifier/9781009157940/type/book**.

3 S. Dangendorf, C. Hay, F. M. Calafat, M. Marcos, C. G. Piecuch and K. Berk, *et al.*, Persistent acceleration in global sea-level rise since the 1960s, *Nat Clim Chang.*, 2019, **9**(9), 705–710.

4 J. E. Halofsky, D. L. Peterson and B. J. Harvey, Changing wildfire, changing forests: the effects of climate change on fire regimes and vegetation in the Pacific Northwest, USA, *Fire Ecol.*, 2020, **16**(1), 4.

5 S. Mansoor, I. Farooq, M. M. Kachroo, A. E. D. Mahmoud, M. Fawzy and S. M. Popescu, *et al.*, Elevation in wildfire frequencies with respect to the climate change, *J. Environ. Manage.*, 2022, **301**, 113769.

6 IPCC, *Climate Change 2022: Mitigation of Climate Change: Summary for Policymakers*, Cambridge University Press, Cambridge, UK and New York, NY, USA, 2022, p. 52. Available from: **https://www.ipcc.ch/report/ar6/wg3/downloads/report/IPCC_AR6_WGIII_SPM.pdf**.

7 International Energy Agency, *Direct Air Capture: A Key Technology for Net Zero*, OECD, Paris, 2022, Available from: **https://www.oecd-ilibrary.org/energy/direct-air-capture_bbd20707-en**.

8 A. Esqué, A. Mitchell, K. Rastogi and R. Riedel, *Decarbonizing the Aviation Sector: Making Net Zero Aviation Possible*, 2022, p. 78, Available from: **https://www.mckinsey.com/~/media/mckinsey/industries/aerospace%20and%20defense/our%20insights/decarbonizing%20the%20aviation%20sector%20making%20net%20zero%20aviation%20possible/making-net-zero-aviation-possible-full-report.pdf?shouldIndex=false**.

9 E. I. Koytsoumpa, C. Bergins and E. Kakaras, The CO_2 economy: Review of CO_2 capture and reuse technologies, *J. Supercrit. Fluids*, 2018, **132**, 3–16.

10 International Energy Agency, *Energy Technology Perspectives 2020-Special Report on Carbon Capture Utilisation and Storage: CCUS in clean energy transitions*, Organisation for Economic Co-operation and Development, Paris, 2020, Available from: **https://www.oecd-ilibrary.org/energy/energy-technology-perspectives-2020-special-report-on-carbon-capture-utilisation-and-storage_208b66f4-en**.

11 C. Song, Q. Liu, S. Deng, H. Li and Y. Kitamura, Cryogenic-based CO_2 capture technologies: State-of-the-art developments and current challenges, *Renewable Sustainable Energy Rev.*, 2019, **101**, 265–278.

12 L. Rosa, D. L. Sanchez and M. Mazzotti, Assessment of carbon dioxide removal potential via BECCS in a carbon-neutral Europe, *Energy Environ. Sci.*, 2021, **14**(5), 3086–3097.

13 J. Fuhrman, H. McJeon, P. Patel, S. C. Doney, W. M. Shobe and A. F. Clarens, Food–energy–water implications of negative emissions technologies in a +1.5 °C future, *Nat Clim Chang.*, 2020, **10**(10), 920–927.

14 S. Roe, C. Streck, M. Obersteiner, S. Frank, B. Griscom and L. Drouet, *et al.*, Contribution of the land sector to a 1.5 °C world, *Nat. Clim. Chang.*, 2019, **9**(11), 817–828.

This journal is © The Royal Society of Chemistry 2023

Energy Environ. Sci., 2023, **16**, 6127–6146 | **6143**

15 S. Uden, P. Dargusch and C. Greig, Cutting through the noise on negative emissions, *Joule*, 2021, **5**(8), 1956–1970.

16 K. Dooley and S. Kartha, Land-based negative emissions: risks for climate mitigation and impacts on sustainable development, *Int. Environ. Agreements*, 2018, **18**(1), 79–98.

17 N. McQueen, K. V. Gomes, C. McCormick, K. Blumanthal, M. Pisciotta and J. Wilcox, A review of direct air capture (DAC): scaling up commercial technologies and innovating for the future, *Prog. Energy*, 2021, **3**(3), 032001.

18 F. Sabatino, A. Grimm, F. Gallucci, M. van Sint Annaland, G. J. Kramer and M. Gazzani, A comparative energy and costs assessment and optimization for direct air capture technologies, *Joule*, 2021, **5**(8), 2047–2076.

19 M. Fasihi, O. Efimova and C. Breyer, Techno-economic assessment of CO_2 direct air capture plants, *J. Cleaner Prod.*, 2019, **224**, 957–980.

20 National Academies of Sciences, Engineering, and Medicine, Direct Air Capture, in *Negative Emissions Technologies and Reliable Sequestration: A Research Agenda*, The National Academies Press, Washington, DC, 2019. Available from: **https://www.nap.edu/read/25259/chapter/7**.

21 C. Beuttler, L. Charles and J. Wurzbacher, The role of direct air capture in mitigation of anthropogenic greenhouse gas emissions, *Front. clim.*, 2019, **1**, 10.

22 G. Realmonte, L. Drouet, A. Gambhir, J. Glynn, A. Hawkes and A. C. Köberle, *et al.*, An inter-model assessment of the role of direct air capture in deep mitigation pathways, *Nat. Commun.*, 2019, **10**(1), 3277.

23 H. Azarabadi and K. S. Lackner, A sorbent-focused techno-economic analysis of direct air capture, *Appl. Energy*, 2019, **250**, 959–975.

24 N. McQueen, P. Psarras, H. Pilorgé, S. Liguori, J. He and M. Yuan, *et al.*, Cost analysis of direct air capture and sequestration coupled to low-carbon thermal energy in the United States, *Environ. Sci. Technol.*, 2020, **54**(12), 7542–7551.

25 O. J. Guerra, H. M. Almajed, W. A. Smith, A. Somoza-Tornos and B. M. S. Hodge, Barriers and opportunities for the deployment of CO_2 electrolysis in net-zero emissions energy systems, *Joule*, 2023, **7**(6), 1111–1133.

26 E. S. Sanz-Pérez, C. R. Murdock, S. A. Didas and C. W. Jones, Direct capture of CO_2 from ambient air, *Chem. Rev.*, 2016, **116**(19), 11840–11876.

27 J. A. Wurzbacher, C. Gebald, N. Piatkowski and A. Steinfeld, Concurrent separation of CO_2 and H_2O from air by a temperature-vacuum swing adsorption/desorption cycle, *Environ. Sci. Technol.*, 2012, **46**(16), 9191–9198.

28 D. W. Keith, G. Holmes, D. St. Angelo and K. Heidel, A process for capturing CO_2 from the atmosphere, *Joule*, 2018, **2**(8), 1573–1594.

29 J. Mertens, C. Breyer, K. Arning, A. Bardow, R. Belmans and A. Dibenedetto, *et al.*, Carbon capture and utilization: More than hiding CO_2 for some time, *Joule*, 2023, **7**(3), 442–449.

30 International Energy Agency, *Section 45Q Credit for Carbon Oxide Sequestration – Policies*, United States, 2023,

Available from: **https://www.iea.org/policies/4986-section-45q-credit-for-carbon-oxide-sequestration**.

31 Trading Economics, 2023 [cited 2023 Mar 15]. EU Carbon Permits. Available from: **https://tradingeconomics.com/commodity/carbon**.

32 M. Li, E. Irtem, H. P. Iglesias van Montfort, M. Abdinejad and T. Burdyny, Energy comparison of sequential and integrated CO_2 capture and electrochemical conversion, *Nat. Commun.*, 2022, **13**(1), 5398.

33 E. W. Lees, M. Goldman, A. G. Fink, D. J. Dvorak, D. A. Salvatore and Z. Zhang, *et al.*, Electrodes designed for converting bicarbonate into CO, *ACS Energy Lett.*, 2020, **5**(7), 2165–2173.

34 T. Li, E. W. Lees, M. Goldman, D. A. Salvatore, D. M. Weekes and C. P. Berlinguette, Electrolytic conversion of bicarbonate into CO in a flow cell, *Joule*, 2019, **3**(6), 1487–1497.

35 A. J. Welch, E. Dunn, J. S. DuChene and H. A. Atwater, Bicarbonate or carbonate processes for coupling carbon dioxide capture and electrochemical conversion, *ACS Energy Lett.*, 2020, **5**(3), 940–945.

36 Y. C. Li, G. Lee, T. Yuan, Y. Wang, D. H. Nam and Z. Wang, *et al.*, CO_2 electroreduction from carbonate electrolyte, *ACS Energy Lett.*, 2019, **4**(6), 1427–1431.

37 P. Debergh, O. Gutiérrez-Sánchez, M. N. Khan, Y. Y. Birdja, D. Pant and M. Bulut, The economics of electrochemical syngas production via direct air capture, *ACS Energy Lett.*, 2023, 3398–3403.

38 M. Moreno-Gonzalez, A. Berger, T. Borsboom-Hanson and W. Mérida, Carbon-neutral fuels and chemicals: Economic analysis of renewable syngas pathways via CO_2 electrolysis, *Energy Convers. Manage.*, 2021, **244**, 114452.

39 Q. Jiang, S. Faraji, D. A. Slade and S. M. Stagg-Williams, Review of Mixed Ionic and Electronic Conducting Ceramic Membranes as Oxygen Sources for High-Temperature Reactors, in *Membrane Science and Technology*, ed. S. T. Oyama and S. M. Stagg-Williams, Elsevier, 2011, Ch. 11-A, vol. 14. pp. 235–273, (Inorganic Polymeric and Composite Membranes). Available from: **https://www.sciencedirect.com/science/article/pii/B9780444537287000112**.

40 V. Rao and W. Vizuete, Alternative fuels, in *Particulates Matter*, ed. V. Rao and W. Vizuete, Elsevier, 2021, Ch. 11, pp. 181–197. (Emerging Issues in Analytical Chemistry). Available from: **https://www.sciencedirect.com/science/article/pii/B9780128169049000234**.

41 O. S. Joo, K. D. Jung, I. Moon, A. Y. Rozovskii, G. I. Lin and S. H. Han, *et al.*, Carbon dioxide hydrogenation to form methanol via a reverse-water-gas-shift reaction (the CAMERE process), *Ind. Eng. Chem. Res.*, 1999, **38**(5), 1808–1812.

42 S. M. Jarvis and S. Samsatli, Technologies and infrastructures underpinning future CO2 value chains: A comprehensive review and comparative analysis, *Renewable Sustainable Energy Rev.*, 2018, **85**, 46–68.

43 J. Puhar, A. Vujanovic, D. Krajnc and L. Cucek, Technology Readiness Level Assessment of Formalin Production Pathways, *Chem. Eng. Trans.*, 2021, **88**, 607–612.

6144 | *Energy Environ. Sci.*, 2023, **16**, 6127–6146

This journal is © The Royal Society of Chemistry 2023

44 A. H. Sahir, Y. Zhang, E. C. D. Tan and L. Tao, Understanding the role of Fischer–Tropsch reaction kinetics in techno-economic analysis for co-conversion of natural gas and biomass to liquid transportation fuels, *Biofuels, Bioprod. Biorefin.*, 2019, **13**(5), 1306–1320.

45 J. G. Speight, 6-Gasification processes for syngas and hydrogen production, in *Gasification for Synthetic Fuel Production*, ed. R. Luque and J. G. Speight, Woodhead Publishing, 2015, pp. 119–146, (Woodhead Publishing Series in Energy). Available from: https://www.sciencedirect.com/science/article/pii/B9780857098023000060.

46 E. Rezaei and S. Dzuryk, Techno-economic comparison of reverse water gas shift reaction to steam and dry methane reforming reactions for syngas production, *Chem. Eng. Res. Des.*, 2019, **144**, 354–369.

47 Z. Ma, S. Kang, J. Ma, L. Shao, A. Wei and C. Liang, *et al.*, High-performance and rapid-response electrical heaters based on ultraflexible, heat-resistant, and mechanically strong aramid nanofiber/Ag nanowire nanocomposite papers, *ACS Nano*, 2019, **13**(7), 7578–7590.

48 S. Nitopi, E. Bertheussen, S. B. Scott, X. Liu, A. K. Engstfeld and S. Horch, *et al.*, Progress and perspectives of electrochemical CO$_2$ reduction on copper in aqueous electrolyte, *Chem. Rev.*, 2019, **119**(12), 7610–7672.

49 R. Küngas, Review—Electrochemical CO$_2$ reduction for CO production: Comparison of low- and high-temperature electrolysis technologies, *J. Electrochem. Soc.*, 2020, **167**(4), 044508.

50 C. Chen, J. F. Khosrowabadi Kotyk and S. W. Sheehan, Progress toward commercial application of electrochemical carbon dioxide reduction, *Chem*, 2018, **4**(11), 2571–2586.

51 M. Jouny, W. Luc and F. Jiao, General techno-economic analysis of CO$_2$ electrolysis systems, *Ind. Eng. Chem. Res.*, 2018, **57**(6), 2165–2177.

52 T. Daniel, A. Masini, C. Milne, N. Nourshagh, C. Iranpour and J. Xuan, Techno-economic analysis of direct air carbon capture with CO$_2$ utilisation, *Carbon Capture Sci. Technol.*, 2022, **2**, 100025.

53 NREL, *H2A: Hydrogen Analysis Production Models*, 2020, Available from: https://www.nrel.gov/hydrogen/h2a-production-models.html.

54 G. Wen, B. Ren, X. Wang, D. Luo, H. Dou and Y. Zheng, *et al.*, Continuous CO$_2$ electrolysis using a CO$_2$ exsolution-induced flow cell, *Nat. Energy*, 2022, **7**(10), 978–988.

55 K. Lackner, H. J. Ziock and P. Grimes, Carbon Dioxide Extraction from Air: Is It An Option?, Los Alamos National Lab. (LANL), Los Alamos, NM (United States); 1999 Feb [cited 2022 Aug 17]. Report No.: LA-UR-99-583. Available from: https://www.osti.gov/biblio/770509-carbon-dioxide-extraction-from-air-option.

56 F. S. Zeman and K. S. Lackner, Capturing carbon dioxide directly from the atmosphere, *World Resource Rev.*, 2004, **16**(2), 157–172.

57 M. Juneau, M. Vonglis, J. Hartvigsen, L. Frost, D. Bayerl and M. Dixit, *et al.*, Assessing the viability of K-Mo$_2$C for

58 S. Adelung, S. Maier and R. U. Dietrich, Impact of the reverse water-gas shift operating conditions on the Power-to-Liquid process efficiency, *Sustain. Energy Technol. Assess.*, 2021, **43**, 100897.

59 D. H. König, N. Baucks, R. U. Dietrich and A. Wörner, Simulation and evaluation of a process concept for the generation of synthetic fuel from CO2 and H2, *Energy*, 2015, **91**, 833–841.

60 E. Schwab, A. Milanov, S. A. Schunk, A. Behrens and N. Schödel, Dry reforming and reverse water gas shift: alternatives for syngas production?, *Chem. Ing. Tech.*, 2015, **87**(4), 347–353.

61 R. I. Masel, Z. Liu, H. Yang, J. J. Kaczur, D. Carrillo and S. Ren, *et al.*, An industrial perspective on catalysts for low-temperature CO$_2$ electrolysis, *Nat. Nanotechnol.*, 2021, **16**(2), 118–128.

62 M. P. L. Kang, M. J. Kolb, F. Calle-Vallejo and B. S. Yeo, The Role of Undercoordinated Sites on Zinc Electrodes for CO$_2$ Reduction to CO, *Adv. Funct. Mater.*, 2022, **32**(23), 2111597.

63 X. Zhang, Z. Wu, X. Zhang, L. Li, Y. Li and H. Xu, *et al.*, Highly selective and active CO$_2$ reduction electrocatalysts based on cobalt phthalocyanine/carbon nanotube hybrid structures, *Nat. Commun.*, 2017, **8**(1), 14675.

64 M. Jouny, G. S. Hutchings and F. Jiao, Carbon monoxide electroreduction as an emerging platform for carbon utilization, *Nat Catal.*, 2019, **2**(12), 1062–1070.

65 F. Sastre, M. J. Muñoz-Batista, A. Kubacka, M. Fernández-García, W. A. Smith and F. Kapteijn, *et al.*, Efficient electrochemical production of syngas from CO$_2$ and H$_2$O by using a nanostructured Ag/g-C$_3$N$_4$ catalyst, *ChemElectroChem*, 2016, **3**(9), 1497–1502.

66 M. B. Ross, Y. Li, P. De Luna, D. Kim, E. H. Sargent and P. Yang, Electrocatalytic rate alignment enhances syngas generation, *Joule*, 2019, **3**(1), 257–264.

67 A. Hauch, R. Küngas, P. Blennow, A. B. Hansen, J. B. Hansen and B. V. Mathiesen, *et al.*, Recent advances in solid oxide cell technology for electrolysis, *Science*, 2020, **370**(6513), eaba6118.

68 Twelve, 2023 [cited 2023 Sep 18]. Twelve. Available from: https://www.twelve.co.

69 Dioxide Materials, 2023 [cited 2023 Sep 18]. Dioxide Materials. Available from: https://dioxidematerials.com/.

70 OCOchem, 2023 [cited 2023 Sep 18]. OCOchem. Available from: https://ocochem.com/.

71 S. A. Grigoriev, V. N. Fateev, D. G. Bessarabov and P. Millet, Current status, research trends, and challenges in water electrolysis science and technology, *Int. J. Hydrogen Energy*, 2020, **45**(49), 26036–26058.

72 O. Schmidt, A. Gambhir, I. Staffell, A. Hawkes, J. Nelson and S. Few, Future cost and performance of water electrolysis: An expert elicitation study, *Int. J. Hydrogen Energy*, 2017, **42**(52), 30470–30492.

73 N. V. Kuleshov, V. N. Kuleshov, S. A. Dovbysh, S. A. Grigoriev, S. V. Kurochkin and P. Millet, Development

This journal is © The Royal Society of Chemistry 2023

Energy Environ. Sci., 2023, **16**, 6127–6146 | **6145**

and performances of a 0.5 kW high-pressure alkaline water electrolyser, *Int. J. Hydrogen Energy*, 2019, **44**(56), 29441–29449.

74 L. Barelli, G. Bidini, F. Gallorini and S. Servili, Hydrogen production through sorption-enhanced steam methane reforming and membrane technology: A review, *Energy*, 2008, **33**(4), 554–570.

75 R. Soltani, M. A. Rosen and I. Dincer, Assessment of CO_2 capture options from various points in steam methane reforming for hydrogen production, *Int. J. Hydrogen Energy*, 2014, **39**(35), 20266–20275.

76 International Energy Agency, *The Future of Hydrogen*, IEA Publications, France, 2019, p. 199.

77 M. H. Ali Khan, R. Daiyan, P. Neal, N. Haque, I. MacGill and R. Amal, A framework for assessing economics of blue hydrogen production from steam methane reforming using carbon capture storage & utilisation, *Int. J. Hydrogen Energy*, 2021, **46**(44), 22685–22706.

78 A. O. Oni, K. Anaya, T. Giwa, G. Di Lullo and A. Kumar, Comparative assessment of blue hydrogen from steam methane reforming, autothermal reforming, and natural gas decomposition technologies for natural gas-producing regions, *Energy Convers. Manage.*, 2022, **254**, 115245.

79 G. Wen, *Nanostructured Materials and Electrodes Engineering for Efficient CO_2 Conversion*, University of Waterloo, Waterloo, Ontario, Canada, 2020. Available from: https://hdl.handle.net/10012/16283.

80 INTRATEC, 2018 [cited 2023 Jul 24]. Hydrochloric Acid Price. Available from: https://www.intratec.us/chemical-markets/hydrochloric-acid-price.

81 ChemAnalyst, Caustic Potash Price Trend and Forecast, 2023 [cited 2023 Jul 14]. Available from: https://www.chemanalyst.com/Pricing-data/caustic-potash-1212.

82 INTRATEC, 2018 [cited 2023 Jul 6]. Oxygen Prices. Available from: https://www.intratec.us/chemical-markets/oxygen-price.

83 Siemens Energy, Silyzer 300, Siemens Energy; [cited 2023 May 8]. Available from: https://assets.siemens-energy.com/siemens/assets/api/uuid:40d117f9-1b4f-4816-ae58-b47cf0-11d406/datasheet-pem-electrolyzer-17-5mw.pdf?ste_sid=102-9cbb79f7d42ba43a3c1a46a35851b.

84 P. Ripson and H. van't Noordende, *Integration of gigawatt scale electrolyser in five industrial clusters: Public summary*, Institute for Sustainable Process Technology, 2020. Available from: https://ispt.eu/media/ISPT-samenvattend-rapport-GigaWatt-online-def.pdf.

85 R. J. Ouimet, J. R. Glenn, D. De Porcellinis, A. R. Motz, M. Carmo and K. E. Ayers, The Role of Electrocatalysts in the Development of Gigawatt-Scale PEM Electrolyzers, *ACS Catal.*, 2022, **12**(10), 6159–6171.

86 R. Kas, A. G. Star, K. Yang, T. Van Cleve, K. C. Neyerlin and W. A. Smith, Along the channel gradients impact on the spatioactivity of gas diffusion electrodes at high conversions during CO_2 electroreduction, *ACS Sustainable Chem. Eng.*, 2021, **9**(3), 1286–1296.

87 B. Pan, J. Fan, J. Zhang, Y. Luo, C. Shen and C. Wang, *et al.*, Close to 90% single-pass conversion efficiency for CO_2 electroreduction in an acid-fed membrane electrode assembly, *ACS Energy Lett.*, 2022, **7**(12), 4224–4231.

88 J. Huber, K. Lohmann, M. Schmidt and C. Weinhardt, Carbon efficient smart charging using forecasts of marginal emission factors, *J. Cleaner Prod.*, 2021, **284**, 124766.

89 NREL, 2023 Annual Technology Baseline (ATB) Cost and Performance Data for Electricity Generation Technologies [data set], Golden, CO. Available from: https://data.openei.org/submissions/5865.

90 G. Towler and R. Sinnott, Capital Cost Estimating, *Chemical Engineering Design*, Elsevier, 2013, pp. 307–354, Available from: https://linkinghub.elsevier.com/retrieve/pii/B9780080966595000079.

91 D. R. Woods, Appendix D: Capital Cost Guidelines, in *Rules of Thumb in Engineering Practice*, John Wiley & Sons, Ltd, 2007, pp. 376–436. Available from: https://onlinelibrary.wiley.com/doi/abs/10.1002/9783527611119.app4.

92 M. Ramdin, B. De Mot, A. R. T. Morrison, T. Breugelmans, L. J. P. van den Broeke and J. P. M. Trusler, *et al.*, Electroreduction of CO_2/CO to C_2 products: Process modeling, downstream separation, system integration, and economic analysis, *Ind. Eng. Chem. Res.*, 2021, **60**(49), 17862–17880, DOI: 10.1021/acs.iecr.1c03592.

93 T. Alerte, J. P. Edwards, C. M. Gabardo, C. P. O'Brien, A. Gaona and J. Wicks, *et al.*, Downstream of the CO_2 electrolyzer: Assessing the energy intensity of product separation, *ACS Energy Lett.*, 2021, **6**(12), 4405–4412.

94 T. Moore, D. I. Oyarzun, W. Li, T. Y. Lin, M. Goldman and A. A. Wong, *et al.*, Electrolyzer energy dominates separation costs in state-of-the-art CO_2 electrolyzers: Implications for single-pass CO_2 utilization, *Joule*, 2023, **7**(4), 782–796.

95 J. P. Edwards, Y. Xu, C. M. Gabardo, C. T. Dinh, J. Li and Z. Qi, *et al.*, Efficient electrocatalytic conversion of carbon dioxide in a low-resistance pressurized alkaline electrolyzer, *Appl. Energy*, 2020, **261**, 114305.

96 U.S. Energy Information Administration, Annual Energy Outlook 2023 – Table 13, 2023 [cited 2023 Jul 13]. Available from: https://www.eia.gov/outlooks/aeo/data/browser/#/?id=13-AEO2023&cases=ref2023&sourcekey=0.

97 D. Salvatore and C. P. Berlinguette, Voltage matters when reducing CO_2 in an electrochemical flow cell, *ACS Energy Lett.*, 2020, **5**(1), 215–220.

98 IHS Markit, *IHS Markit Process Economics Program (PEP) Yearbook*, 2021.

99 O. J. Guerra, J. Eichman and P. Denholm, Optimal energy storage portfolio for high and ultrahigh carbon-free and renewable power systems, *Energy Environ. Sci.*, 2021, **14**(10), 5132–5146.

100 O. J. Guerra, J. Eichman, J. Kurtz and B. M. Hodge, Cost competitiveness of electrolytic hydrogen, *Joule*, 2019, **3**(10), 2425–2443.

101 United Nations, 2023 [cited 2023 Jun 28]. THE 17 GOALS | Sustainable Development. Available from: https://sdgs.un.org/goals.

102 P. Gabrielli, L. Rosa, M. Gazzani, R. Meys, A. Bardow and M. Mazzotti, *et al.*, Net-zero emissions chemical industry in a world of limited resources, *One Earth*, 2023, **6**(6), 682–704.

103 Worldometer, [cited 2023 Sep 10]. Water Use Statistics. Available from: https://www.worldometers.info/water/.

6146 | *Energy Environ. Sci.*, 2023, **16**, 6127–6146

This journal is © The Royal Society of Chemistry 2023